

The Further Development of Fringe Electric Field Theory for the Design of a Vertical Comb Drive to be used as a Force-Compensation Mechanism in an Interfacial Force Microscope

by

Else Elizabeth Gallagher

A thesis submitted in partial fulfillment of the requirements for the degree of

Doctor of Philosophy

Department of Mechanical Engineering  
University of Alberta

© Else Elizabeth Gallagher, 2015

# Abstract

The overall objective of the research presented here is to begin the design of a comb drive that is to be used as a force-compensation mechanism in an interfacial force microscope. More specifically, the objective of this research is to choose the type of comb drive that has the most potential to further the measurement of interfacial forces, and fabricate test specimens of such comb drives that are then used in two studies that are intended to confirm, at least in part, that comb drives have potential to aid in the measurement of interfacial forces, and to further develop the electrostatic theory used to design comb drives in general. In the first study, the lower limit of the spring stiffness that comb drives can easily be fabricated with is explored, as the mechanical resistance they provide will affect the sensitivity of the force-compensation system. The objective of the second study is to examine how the fringe electric fields around the comb teeth (and thus more of the dimensions of the comb teeth) should be included in the calculation of the electrostatic force between the teeth so that the performance of the comb drives may be predicted more accurately.

Comb drives are an attractive type of force-compensator because they can be made out of common materials and their electrodes can be automatically aligned with each other during their manufacture. This research focuses on comb drives that have springs that are designed to be compliant in the direction perpendicular to the substrate they are machined on (or vertically) rather than in the direction parallel to the substrate (or laterally), as vertically-oriented springs can be fabricated with a lower stiffness more easily. Vertically-offset comb teeth are designed to complement such springs so that electrostatic forces can be applied to the movable combs in both the upwards and downwards directions, and thus both attractive and repulsive interfacial forces

on a probe attached to the movable combs can be compensated for. This research further focuses on vertical comb drives that have opposing comb teeth that are offset by a constant amount along their length, without a ground plane, so that a basic geometry can be considered for the modelling of the electric fields around them.

A simple process that can produce comb drives capable of bi-directional vertical electrical actuation was chosen from the literature that created the vertical offset between its combs by etching down the tops of some of their teeth. It was learned that this could be done using only photoresist to mask the rest of the teeth, which had the advantage of protecting the sides of the teeth as well as their tops during the etch.

The lower limit of the spring stiffness that the comb drives could be fabricated with was explored by fabricating several comb drives with different spring designs and applying loads to their movable combs through a series of weights and voltages, and measuring the resulting displacements of their springs. The comb drives with the lowest spring stiffnesses are promising candidates for aiding in measuring interfacial forces.

Traditionally, an estimate of the net electrostatic force in comb drives that does not include the fringe electric fields around the tops and bottoms of their teeth has been used to choose the dimensions of the teeth. The electrostatic forces in several fabricated comb drives were thus measured – again by measuring the displacements of their movable combs as voltages were applied to them, after the stiffnesses of their corresponding springs had been determined. The results are compared to mathematical models of the fringe electric fields of increasing complexity to estimate the amount of complexity required for an accurate prediction of the electrostatic force.

The measurement of the electrostatic forces in the fabricated comb drives also indicated that the current design will only generate about half of the electrostatic force for any given voltage than that predicted by a model that does not include the fringe fields around the comb teeth.

# Preface

Chapter 3 of this thesis was published in 2012 as “A review of fabrication processes for vertical comb drives” by Else Gallagher, Walied Moussa, and Mark McDermott in *Microsystem Technologies*. Else Gallagher was responsible for identifying the need for summarizing and comparing such fabrication processes, finding the processes in the literature, choosing the criteria on which the comparisons are based, and composing the manuscript. Dr. McDermott contributed to manuscript edits.

Chapters 2, 4, and 5 of this thesis were published in 2014 as “A preliminary investigation of the potential mechanical sensitivity of vertical comb drives” by Else Gallagher and Walied Moussa in the *Journal of Micromechanics and Microengineering*. Else Gallagher was responsible for identifying the advantages of using vertical comb drives to measure interfacial forces, modifying the fabrication process taken from the literature to produce the comb drives used in the experimental studies, identifying the need to test the lower limit of the spring stiffnesses the comb drives could be easily fabricated with, designing the procedure by which the spring stiffnesses were measured, collecting and interpreting the data, and composing the manuscript. Dr. Moussa contributed to manuscript edits.

Chapter 6 of this thesis was published in 2014 as “A study of the effect of the fringe fields on the electrostatic force in vertical comb drives” by Else Gallagher and Walied Moussa in *Sensors*. Else Gallagher was responsible for verifying the accuracy of the finite element models used against two different analytical models found in the literature, measuring the electrostatic forces in the fabricated vertical comb drives, comparing the measured electrostatic forces to those predicted with various mathematical models in order to estimate the amount of complexity required in the models to make accurate predictions of the electrostatic forces, and composing the manuscript. Dr. Moussa contributed to manuscript edits.

This work is dedicated to all of the people who were integral to it, that other forms of acknowledgement do not cover.

It is dedicated to the Nanofab staff, both past and present, and particularly to Scott, for all the times he fetched the broken pieces of my wafers out of the plasma etchers, and to Glenn, for all the times he fetched my stray die out of the inner workings of the dicing saw.

It is dedicated to Farshid, for giving me the idea to look into how the fringe fields around parallel plates affect the electrostatic forces between them, and to Mike, for giving me the idea to double-check the accuracy of the optical profilometer.

It is dedicated to my friends, particularly those in the circus, for helping me keep things in perspective.

Finally, it is dedicated to my mom, my dad, and my sister, for their unending support, and to my lead henchman, for telling me that I did not have to go back to school – which, of course, made me realize that I wanted to.

## **Acknowledgements**

The author would like to thank Dr. Munoz-Paniagua for numerous discussions regarding the design of interfacial force microscopes, and Dr. Henry van Roessel for an invaluable discussion regarding elliptic functions. She would also like to acknowledge that the comb drives used in these studies she fabricated in the University of Alberta Nanofab, with the financial assistance of the CMC MNT program. The author would like to express her gratitude to Mr. Twanow for allowing her access to the optical profilometer. Finally, the author would like to thank the National Research Council Canada – National Institute for Nanotechnology, the Natural Sciences and Engineering Research Council of Canada, the Auto21 Network, the Department of Chemistry at the University of Alberta, and Micralyne for funding this work.

# Table of Contents

Chapter 1 : Introduction .....	1
1.1 Research Objectives and Methods Employed.....	1
1.2 Thesis Overview .....	2
Chapter 2 : Background .....	3
2.1 Comb Drives .....	3
2.2 Comb Drives as Force-Compensation Mechanisms .....	4
2.3 Vertical vs. Lateral Comb Drives for Measuring Interfacial Forces .....	5
Chapter 3 : A Review of Fabrication Processes for Vertical Comb Drives.....	10
3.1 Common Characteristics of Vertical Comb Drives .....	11
3.1.1 Structural Materials.....	11
3.1.2 Allowable Design Versatility.....	12
3.1.3 Trimming of Springs and Teeth.....	12
3.1.4 Horizontal Alignment between Fixed and Movable Combs.....	13
3.2 Comparison of Fabrication Processes .....	14
3.2.1 Displaced Anchor Processes .....	14
3.2.2 Single Wafer Processes.....	16
3.2.2.1 (111) Single Wafer Process .....	16
3.2.2.2 (100) Single Wafer Process .....	17
3.2.2.3 BELST II Process .....	17
3.2.3 Polysilicon Trench Re-Fill Processes .....	18
3.2.3.1 Polysilicon Trench Re-Fill Process with an Upper Etch-Stop Layer .....	19
3.2.4 Custom SOI Wafer Processes .....	20
3.2.4.1 Custom Double SOI Wafer Process.....	21
3.2.4.2 Bulk Oxidation Process .....	21
3.2.4.3 Custom Double SOI Process with Thinned Springs.....	22
3.2.4.4 Stacked Device Layer Process .....	22
3.2.5 SOI Wafer Processes.....	23
3.2.5.1 Double SOI Wafer Process .....	23
3.2.5.2 Doubled SOI Process .....	23
3.2.5.3 Epipoly Layer Process .....	24
3.2.5.4 Full SOI Wafer Process .....	24

3.2.5.5 Custom Thinned SOI Process .....	25
3.2.5.6 Thinned Handle Wafer Process .....	25
3.2.5.7 Thinned Handle and Springs Process .....	26
3.2.6 Single Device Layer Processes .....	27
3.2.6.1 Simple SOI Process.....	27
3.2.6.2 Custom SCS Layer Process .....	27
3.2.6.3 Partially-Exposed Photoresist Process.....	28
3.2.7 Multiple Wafer Processes .....	28
3.2.7.1 Flipped Chip Process .....	28
3.2.7.2 Parts-Transfer Process .....	29
3.3 Summary and Recommendations .....	29
Chapter 4 : Fabrication of Vertical Comb Drive Prototypes .....	36
4.1 Fabrication Process Steps .....	36
4.2 A Note on Lithography .....	38
Chapter 5 : A Preliminary Investigation of the Potential Mechanical Sensitivity of Vertical Comb Drives.....	41
5.1 Prototype Description .....	41
5.2 Spring Stiffness Predictions.....	42
5.3 Spring Stiffness Measurements.....	42
5.3.1 Characterization of the Stiffest Springs .....	43
5.3.1.1 Lever Method.....	43
5.3.1.2 Direct Method .....	44
5.3.2 Characterization of the Weaker Springs .....	44
5.4 Discussion of Results.....	45
Chapter 6 : A Study of the Effect of the Fringe Fields on the Electrostatic Force in Vertical Comb Drives.....	51
6.1 Derivation of Basic Electrostatic Force Equation.....	51
6.2 First Estimate of the Effect of the Fringe Fields on the Electrostatic Force.....	52
6.3 Addition of Tooth Width to Electrostatic Force Calculations .....	56
6.3.1 Verification of Finite Element Models .....	56
6.3.2 Addition of Width to Plate Model .....	56
6.4 Electrostatic Force Measurements .....	57
6.5 Addition of End of Row to Model.....	60

6.6 Discussion of the Significance of Including the Fringe Fields in the Electrostatic Force Calculation .....	61
Chapter 7 : Conclusions .....	71
7.1 Future Work .....	73
References .....	74

## List of Tables

Table 3.1: A comparison of fabrication processes for vertical comb drives. ....	33
Table 5.1: The predicted and measured stiffnesses of the three spring designs. ....	47

# List of Figures

Figure 2.1: A vertical comb drive. Because the centrelines of the fixed teeth are below those of the movable teeth, when a voltage difference is applied between them the movable teeth will displace downwards, into the substrate. .... 8

Figure 2.2: A lateral comb drive. .... 9

Figure 3.1: Schematics of a multi-functional vertical comb drive, made using a process very similar to the custom SCS layer process [77]. The movable part of the comb drive can be made to tilt back and forth because the fixed combs on either side of the springs are separate from each other. The movable part of the comb drive can also be electrostatically pulled both upwards and downwards because some of the movable combs are the upper combs and some of them are the lower combs. Also, some of the movable combs have no vertical offset from their opposing fixed combs, so when a voltage difference is applied to them they can cause the comb drive to move horizontally. .... 32

Figure 3.2: Many fabrication processes for vertical comb drives create the vertical offset between the centrelines of their opposing comb teeth by etching the tops of their bottom teeth down and the bottoms of their top teeth up. If these partial etches into the structural layer are shallow enough, they can both be done in the same area, so that the thickness of the springs is equal to the vertical overlap between the comb teeth. .... 35

Figure 3.3: A schematic of the cross-section of a structural layer as it undergoes two etches while the masking layers protecting certain regions of it are sequentially removed. In Step 3, the top of what will be the lower structure is etched down as the etch through the structural layer is completed. During this etch the bottom masking layer continues to protect what will be the upper structure. .... 35

Figure 4.1: A vertical comb drive that has two different sets of opposing comb pairs. One set has its fixed combs positioned above the movable combs; the other set has its fixed combs below the movable combs. .... 39

Figure 4.2: A test-etch of the comb teeth into a scrap wafer. Because only the tops of the upper teeth were masked while the tops of the lower teeth were etched down – and the sides of the teeth were not protected – the tops of the lower teeth have been bevelled. .... 39

Figure 4.3: A schematic of a simplified cross-section of a die showing the fabrication process steps followed. .... 40

Figure 5.1: The three spring designs studied. The comb drives were designed to have one of these on each side of the movable combs. The thickness of the narrow spring beams,  $2a_s$ , was equal to the thickness of the device layer. .... 47

Figure 5.2: The mechanism used to apply different weights to the movable combs of the comb drives with the stiffest springs. .... 48

Figure 5.3: The comparison of the displacements of the movable combs to the weights that were applied to them, from which the spring constants of the stiffest springs were calculated. A few

of the data points have been made larger to indicate that those values of the weights were recorded two or three times.....	48
Figure 5.4: Comparisons of the displacements of the movable combs to the electrostatic forces that were applied to them, from which the spring constants of the (a) second-weakest, and (b) weakest springs were calculated. ....	49
Figure 5.5: The scalloped sidewalls left by the Bosch process on the narrowest spring beams..	50
Figure 6.1: Some of the dimensions of the comb teeth that are expected to affect the electrostatic forces generated between them. (b) is an enlarged view of the area indicated in (a). It should be noted that “ $t_S$ ” refers to the thickness of the shorter teeth and “ $t_T$ ” to the thickness of the taller teeth, regardless of which are the fixed teeth and which are the movable teeth.....	63
Figure 6.2: Two different representations of the two-dimensional model of the space between opposing teeth of negligible width.....	63
Figure 6.3: Different predictions of the fraction of the maximum electrostatic force that acts on the movable combs over their displacement. ....	64
Figure 6.4: One of the finite element models that includes the width of the comb teeth. ....	64
Figure 6.5: The first comb drive fabricated for this study. ....	65
Figure 6.6: The relative tooth dimensions of the comb drive in figure 6.5. ....	66
Figure 6.7: A comparison of two different predictions of the electrostatic force to that measured in the vertical comb drive shown in figures 6.5 and 6.6 that has tooth dimensions of $w/t_T=0.260$ , $g/t_T=0.276$ , and $t_S/t_T=0.384$ . The electrostatic forces have been non-dimensionalized with respect to (6.4). (a) shows the measured force calculated from the spring stiffness determined using the lever mechanism; (b) shows the measured force calculated from the spring stiffness determined with the scale mounted on the stage of the optical profilometer. ....	67
Figure 6.8: The measured spring constants of the three vertical comb drive designs. (a) shows the spring stiffnesses determined using the lever mechanism. A few of the data points have been made larger to indicate that those values of the weights were recorded two or three times. (b) shows the spring stiffness determined with the scale mounted on the stage of the optical profilometer.....	68
Figure 6.9: The vertical comb drive design that has its “fixed” combs also attached to springs so that they can be pushed down with the electrical probes to allow the electrostatic forces between the fixed and movable teeth to be measured over a larger range of vertical offsets.....	69
Figure 6.10: Comparisons of three different predictions of the electrostatic forces to those measured in a vertical comb drive that has shorter movable teeth than fixed teeth (with tooth dimensions of $w/t_T=0.241$ , $g/t_T=0.296$ , and $t_S/t_T=0.365$ ). The electrostatic forces have been non-dimensionalized with respect to (6.4). (a) shows the measured forces calculated from the spring stiffness determined using the lever mechanism; (b) shows the measured forces calculated from the spring stiffness determined with the scale mounted on the stage of the optical profilometer.	69
Figure 6.11: Comparisons of three different predictions of the electrostatic forces to those measured in a vertical comb drive that has fixed and movable teeth of the same size ( $w/t_T=0.234$ , $g/t_T=0.300$ , and $t_S/t_T=1$ ). The electrostatic forces have been non-dimensionalized with respect to	

(6.4). (a) shows the measured forces calculated from the spring stiffness determined using the lever mechanism; (b) shows the measured forces calculated from the spring stiffness determined with the scale mounted on the stage of the optical profilometer. .... 70

Figure 6.12: (a) One of the models of a row of teeth with a portion of the device layer at the end. The equipotential lines show the electric field being pulled away from the tops of the shorter teeth, lessening the effect of the width of the teeth on the electrostatic force between them. (b) The corresponding unit comb drive. .... 70

# Chapter 1 : Introduction

## 1.1 Research Objectives and Methods Employed

The overall objective of the research presented here is to begin the design of a comb drive that is to be used as a force-compensation mechanism in an interfacial force microscope. More specifically, the objective of this research is to choose the type of comb drive that has the most potential to further the measurement of interfacial forces, and fabricate test specimens of such comb drives that are then used in two studies that are intended to confirm, at least in part, that comb drives have potential to aid in the measurement of interfacial forces, and to further develop the electrostatic theory used to design comb drives in general. In the first study, the lower limit of the spring stiffness that comb drives can easily be fabricated with is explored, as the mechanical resistance they provide will affect the sensitivity of the force-compensation system. The objective of the second study is to examine how the fringe electric fields around the comb teeth (and thus more of the dimensions of the comb teeth) should be included in the calculation of the electrostatic force between the teeth so that the performance of the comb drives may be predicted more accurately.

The type of comb drive that is used in the studies was chosen by comparing its potential mechanical sensitivity to that of other types of comb drives, as well as its versatility (a force-compensation mechanism should be equally capable of opposing both attractive and repulsive interfacial forces). Because the electric fields within that type of comb drive were to be studied, the most basic comb arrangement that fit the above criteria was also chosen. Test specimens were fabricated following a simple process that had been found in the literature that was determined to be able to produce the required type of comb drive. The fabrication process was modified from its original version to better protect the designed dimensions of the comb teeth during their manufacture. The lower limit of the spring stiffness that the comb drives could be fabricated with was explored by fabricating several comb drives with different spring designs and measuring the displacements of their movable combs as loads were applied to them through a series of weights and voltages. The proper prediction of the net electrostatic force within the comb drives was examined by measuring the electrostatic forces in several fabricated comb

drives – again by measuring the displacements of their movable combs as voltages were applied to them, after the stiffnesses of their corresponding springs had been determined – and comparing the results to mathematical models of the electrostatic force of increasing complexity.

## **1.2 Thesis Overview**

The following chapters detail the work that has thus far been conducted on designing a comb drive that is to be used as a force-compensation mechanism in an interfacial force microscope. Chapter 2 gives the background of this research, explaining what comb drives are, what interfacial forces are, what role force-compensation mechanisms play in measuring interfacial forces, what advantages comb drives would have over other types of force-compensation mechanisms for measuring interfacial forces, and finally, what types of comb drives this research focuses on and why. Chapter 3 reviews a number of fabrication processes for comb drives that were found in the literature. It explains the criteria on which they are compared, and summarizes the fabrication techniques they involve so that the simplest can be chosen that has the capability to produce the type of comb drive required. Chapter 4 details the fabrication process followed to produce the comb drives that the measurements were taken from in the later chapters. Chapter 5 details the measurements taken of the spring stiffnesses of the fabricated comb drives. Chapter 6 details the measurements taken of the electrostatic forces within the fabricated comb drives, as well as the four predictions of the electrostatic forces that the measurements are compared to. Chapter 7 summarizes the conclusions made in the previous chapters.

# Chapter 2 : Background

## 2.1 Comb Drives

Comb drives, as shown in figures 2.1 and 2.2, are electrostatic microactuators in microelectromechanical systems (MEMS) that are comprised of arrays of parallel plates arranged into opposing comb pairs, where one comb in each pair is rigidly fixed to the substrate (and referred to as the fixed comb), and the other comb is fixed to the substrate through a spring structure (and referred to as the movable comb). When a voltage difference is applied between the fixed and movable combs the electrostatic forces generated between them attract the movable combs towards the fixed combs. The research presented here focuses on comb drives that have their plates (or teeth) staggered such that each movable tooth is laterally equidistant from two fixed teeth. In this case, the net electrostatic force on each movable tooth pulls it in between the fixed teeth – parallel to the fixed teeth. When the voltage difference is removed the springs restore the movable combs to their original positions.

Comb drives are often used as micromotors and micropositioners [1, 2]. Frequently they are employed to position micromirrors [1, 3-20], often being fitted with torsion springs, while their fixed and movable comb pairs are positioned on either side of a mirror so that they may apply a force to one edge of the mirror or the other as voltage differences are applied between the combs of one pair at a time. Actuating optical switches, attenuators, or scanners [1, 3-12, 14-21], comb drives can be used to obstruct a beam of light coming from optical fibres, or to steer a beam of light in a one- or two-dimensional space. These abilities can be useful in applications such as laser printing, barcode reading, laser machining, and laser projection displays – as well as in optical communications networks [5, 8, 11, 15, 16, 18-20]. They can also be useful in portable confocal microscopes that can be used *in vivo* for early detection of cancers [17, 18], and for guided precision surgery [18]. Rotatable mirrors can also assist telescopes in tracking fast-moving light sources [16].

If such mirrors are arranged into arrays they can act as wavelength-selective switches or crossconnects [8, 13, 22]. Diffraction gratings and pinholes can also be actuated by comb drives, and the focal planes of microlenses can be controlled [9]. If connected to a circuit that can measure the change in capacitance produced by the variance in overlapping area between their

fixed and movable teeth as an external force is applied to the movable combs, comb drives can also be used as sensors – such as accelerometers [21, 23, 24]. If the circuit is designed to combine their actuation and sensing capabilities they can be used as gyroscopes [21], and a wide variety of transducers [25].

## **2.2 Comb Drives as Force-Compensation Mechanisms**

The focus of this research is on the potential of comb drives to be used as force-compensation mechanisms in interfacial force microscopes. Measuring interfacial forces – the forces that arise between the surfaces of a probe and sample as they are brought together and/or drawn apart, due to phenomena such as adhesion or electric fields [26, 27] – is often done with a mechanism attached to the probe that provides a variable restoring force on it so that its distance from the sample is not affected by the forces it is measuring. Mechanical springs, such as the cantilevers attached to the probes in atomic force microscopes, can be used to measure interfacial forces – if their stiffness is known the force can be determined from their deflection. However, measuring interfacial forces in this manner limits the distances from the sample at which they can be measured, since the force gradient between the probe and sample will draw the probe through it until a position is reached where it balances the restoring force exerted by the spring [28]. For a comb drive to be used as a force-compensation mechanism in an interfacial force microscope, the probe would be attached to its movable combs, and their position would be monitored for any change – most likely with an interferometer or through variations in capacitance. When any displacement of the movable combs is detected, a feedback circuit would apply a voltage difference between the movable combs and the fixed combs so that the electrostatic force generated between them would balance the interfacial force felt by the movable combs. The magnitude of the interfacial force would then be inferred from the magnitude of the voltage used to balance it.

Force-compensation mechanisms for measuring interfacial forces have been added to atomic force microscopes. In some cases a permanent magnet has been attached to the tip of the cantilever while a current has been run through a coil positioned near it, creating a magnetic field around the cantilever [29-36]. In other cases a magnetostrictive film has been deposited on top of the cantilever, which exerts a bending moment on it as the film changes its length under a similarly-applied magnetic field [37]. A piezoelectric film on the cantilever will also change its

length under an applied voltage [38], and the effective stiffness of conductive cantilevers can be controlled by varying the voltage on electrodes positioned near them [39-41].

Other force-compensation mechanisms in interfacial force microscopes have taken the form of “teeter-totter” arrangements – where the probe is attached to one end of a conductive plate that is suspended a short distance away from two fixed conductive plates. The movable plate can be supported by torsion springs [27, 42, 43] or by rigid beams or balls held in place by gravity or a magnetic field [44-46]. Voltage differences between the fixed plates and the movable plate are then varied to create electrostatic restoring forces on the movable plate to oppose the interfacial forces exerted on the probe.

A comb drive can be made out of common conductive and insulating materials, rather than magnetostrictive alloys, or piezoelectric compounds. The electrodes in comb drives can also be automatically aligned with each other during their manufacture, as the final shapes of the teeth can be etched opposite each other in the same wafer at the same time. This should make the relationship between the electrostatic restoring force and the applied voltage more predictable from device to device. A further variation on the “teeter-totter” scheme [47] replaces the conductive plates with pairs of combs. However, movable combs that are suspended by a single torsion spring will be prone to having a certain tilt angle with respect to the fixed combs, which will make predicting the force-voltage relationship between the comb teeth more complicated.

In order to keep the sensitivities of the comb drives fabricated for this work competitive with other force-compensation mechanisms in interfacial force microscopes, they were designed with the aim of resolving forces in the range of 10nN, 100pN [48], and 10pN [49]. They were also designed to have the position of their movable combs monitored with an interferometer that could detect displacements as small as 1Å [50].

### **2.3 Vertical vs. Lateral Comb Drives for Measuring Interfacial Forces**

One aspect of the design of an interfacial force microscope that affects its sensitivity is the stiffness of the springs its probe is attached to. The weaker the springs, the smaller the force that is required on the probe for it to reach the displacement detection limit of the feedback control circuit [51]. The simplest way to fabricate springs for comb drives is to etch a single pattern into the substrate or a layer on the substrate. This method tends to limit springs that provide restoring forces parallel to their substrate (or laterally) to be comprised of “fixed-guided” type beams, such as those shown in figure 2.2. Springs that provide restoring forces perpendicular to their

substrate (or vertically), on the other hand, can be made with the “I”-shaped springs [52] shown in figure 2.1. These “I” springs are comprised of four narrow beams that undergo torsion as one end of the rigid beam between them rises and falls with the movable combs. In general, the overall spring constant,  $k_y$ , for a pair of simple “fixed-guided” beams attached to a movable comb can be described with (2.1), and the overall spring constant,  $k_z$ , for a pair of “I” springs can be described with (2.2):

$$k_y = \frac{2E(2a_s)(2b_s)^3}{L_b^3} \quad (2.1)$$

$$k_z = \frac{8G a_s b_s^3}{L_s L_b^2} \left[ \frac{16}{3} - 3.36 \frac{b_s}{a_s} \left( 1 - \frac{b_s^4}{12a_s^4} \right) \right] \quad (2.2)$$

where  $E$  is the modulus of elasticity of the spring material,  $G$  is the bulk shear modulus,  $2a_s$  and  $2b_s$  are the cross-sectional dimensions of the bending/twisting spring beams (where  $a_s > b_s$ ),  $L_b$  is the largest dimension of the springs (the length of the “fixed-guided” beams, and the length of the rigid beam in the “I” springs – measured between the centre points of the narrow beams), and  $L_s$  is the length of the narrow beams in the “I” springs.

The length of the most delicate beam in the “fixed-guided” springs is thus  $L_b$ , and the length of the most delicate beams in the “I” springs is  $L_s$ . Shorter beams are less prone to breaking during the release of the movable parts of the comb drives from the substrate in the final steps of a fabrication process, and are more rigid in the other directions the movable combs are not intended to move in. Increasing the length of the rigid middle beam in an “I” spring, which can only be made for motion perpendicular to the substrate it is machined on, can lower the spring constant of the spring without increasing the length of the delicate torsion beams. For example, if the springs are etched from single-crystal (100) silicon, and oriented along the crystal planes such that  $E$  and  $G$  are minimized (so the springs with the “fixed-guided” beams are oriented in the  $\langle 100 \rangle$  direction, and the “I” springs are oriented at  $45^\circ$  to that direction), it can be seen that for the same spring constant, the same cross-sectional dimensions of the delicate beams, and the same largest dimension of the springs,  $L_s < L_b$ . In particular,  $L_b = 2.04L_s$  for  $2a_s/2b_s = 10$  (where  $E = 130.2\text{GPa}$  and  $G = 51.2\text{GPa}$ ) and  $L_b = 3.66L_s$  for  $2a_s/2b_s = 1$  (where  $E = 130.2\text{GPa}$  and  $G = 63.2\text{GPa}$ ) [53], which reasonable cross-sectional dimensions are likely to fall

between. This research will therefore focus on developing “I”-shaped springs for comb drives that are to be used as force-compensation mechanisms in interfacial force microscopes.

The movable comb teeth attached to such springs do not need to be offset from their opposing fixed teeth in the vertical direction in order to compensate for interfacial forces in the vertical direction – laterally-offset movable comb teeth will undergo levitation in the presence of a ground plane [54]. However, if the opposing comb teeth are fabricated to be offset from each other in the vertical direction they can be arranged in such a way as to generate electrostatic forces on the movable combs in both the upwards and downwards directions – to provide compensation for both attractive and repulsive interfacial forces. Hence this research will focus on developing vertically-offset comb pairs to go with vertically-oriented springs.

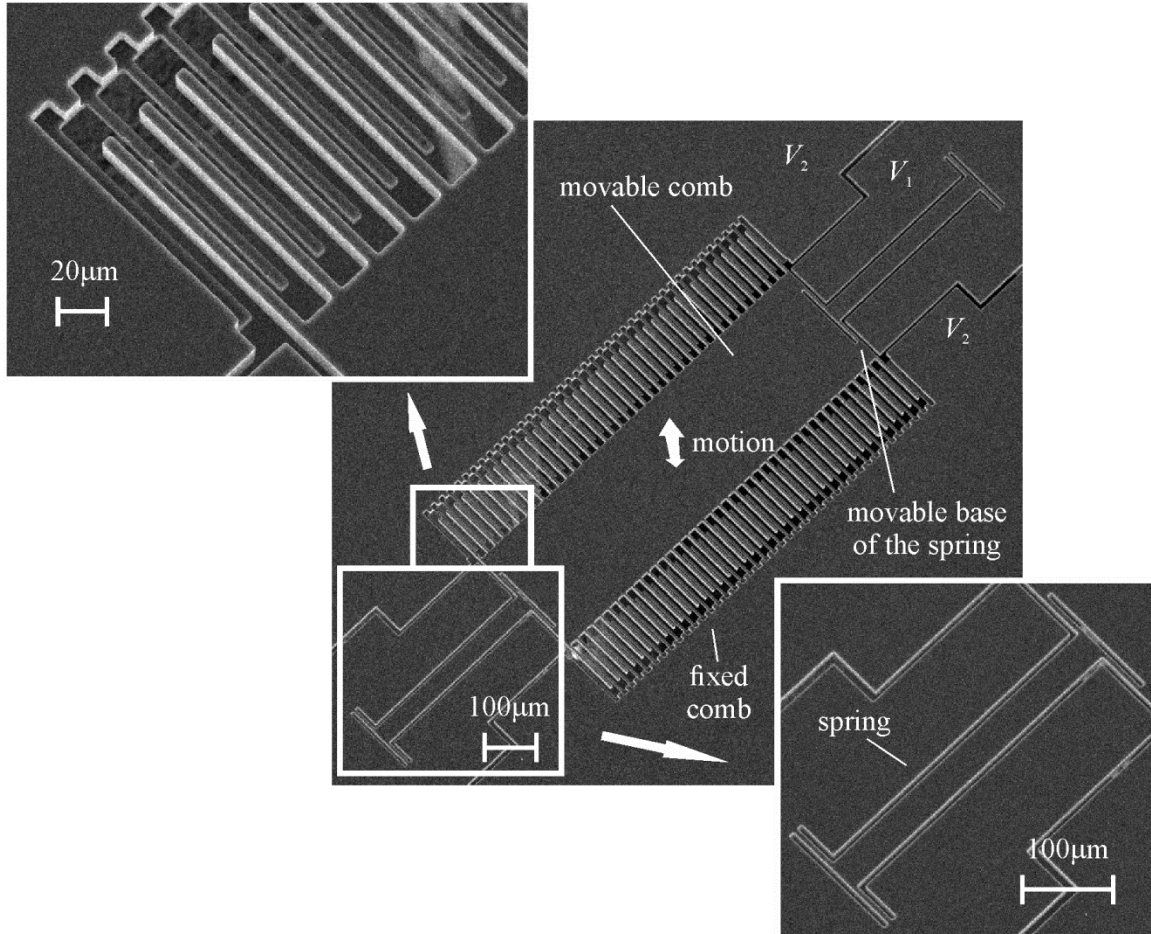


Figure 2.1: A vertical comb drive. Because the centrelines of the fixed teeth are below those of the movable teeth, when a voltage difference is applied between them the movable teeth will displace downwards, into the substrate.

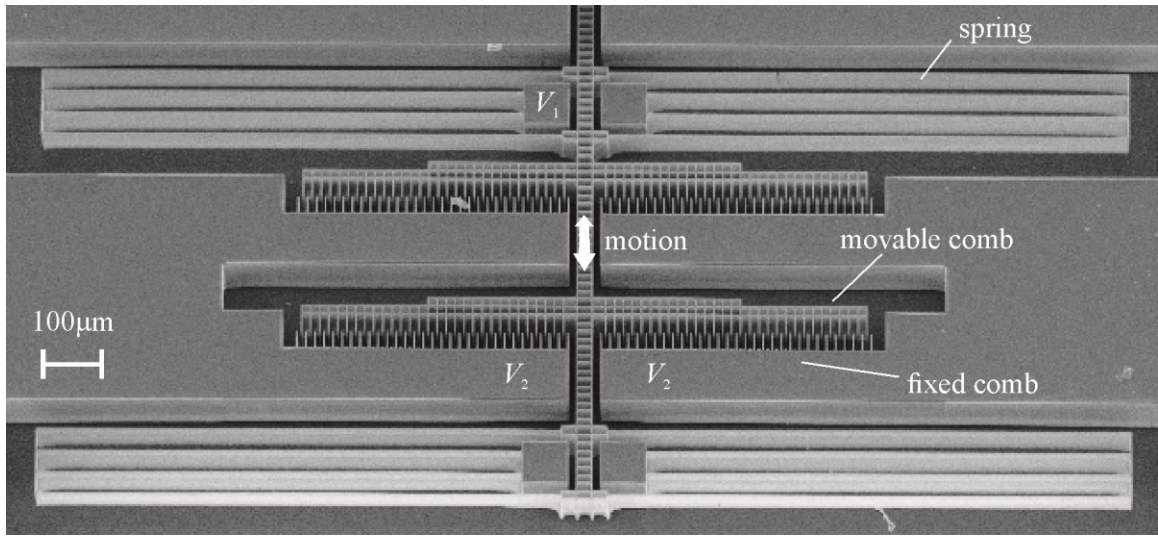


Figure 2.2: A lateral comb drive.

# **Chapter 3 : A Review of Fabrication Processes for Vertical Comb Drives**

While comb drives can be made on the meso-scale [55], force-compensation mechanisms that are small enough to be easily used with an optical microscope allow the choice of the area on a sample surface of where the interfacial forces are to be measured. However, if test specimens are needed for the study of the properties of vertical comb drives, vertical comb drives may not actually need to be fabricated at all. Instead, lateral comb drives can be machined with fixed combs that are also tethered to the rest of the substrate through a spring structure, as with the movable combs. A mechanical probe can then be used to push on the fixed combs to create the vertical offset between them and the movable combs for the duration of the study [56]. If, however, it is necessary to fabricate vertical comb drives, there are many different fabrication processes to choose from. Each have their own advantages that depend on the application they are intended for. Some fabrication processes are patented or are on their way to being patented [57-65]. This chapter reviews 23 processes that have been proposed recently in the literature, specifically for the type of vertical comb drives with fixed and movable combs that are vertically offset by a constant amount along the length of their comb teeth. Fabrication processes for other types of comb drives, involving some very different process techniques than those summarized here, are left for other reviewers to compare.

What follows are brief descriptions of the vertical comb drive fabrication processes, that are intended to assist a designer in choosing processes (or parts of processes from which new ones can be created) that are compatible with whatever micromachining facilities are most easily accessible. Some recommendations are made regarding which of the processes would be the simplest to perform for various applications. Further comparisons between the processes are based on the types of vertical comb drives they can produce, and on characteristics common to all vertical comb drives: how the processes create the vertical offset between their opposing combs, how they electrically isolate their opposing combs, and how they align their opposing combs with each other in the horizontal direction. Also what materials the springs and teeth of the comb drives are made out of is examined, as well as the versatility of the processes – whether they can set the vertical overlap of the opposing teeth, and/or the thickness of the springs

separately from that of the teeth, and whether they can produce comb drives with additional directions of actuation. The importance of these characteristics will be explained in terms of how they affect the performance of the comb drives.

### **3.1 Common Characteristics of Vertical Comb Drives**

The following four sections describe some of the fundamental characteristics common to all vertical comb drives. The fabrication processes summarized in this paper will be compared based on these characteristics, as well as the more obvious ones of how each process achieves electrical isolation between the fixed and movable combs, and how each process produces a vertical offset between the fixed and movable combs. The next four sections will explain: 1) some advantages and disadvantages of the common structural materials used in comb drives, 2) the advantages of having multiple separate fixed combs offset in different directions from the movable portion of a comb drive, 3) why one might want to be able to control the initial vertical overlap between the comb teeth, and the thickness of the springs separately from the thickness of the teeth, and 4) the importance of aligning the fixed and movable teeth with each other in the horizontal direction.

#### ***3.1.1 Structural Materials***

Usually comb drives are made of silicon, a semi-conducting material that can be implanted with other atoms to increase its conductivity, and a common structural material used in the machining of MEMS. Silicon usually comes in either its single-crystalline or polycrystalline form – the former being grown from molten silicon and ground into a wafer before regular micromachining is performed on it, and the later being grown from a gaseous hydrogen compound during the regular micromachining of a wafer.

The micromachining of polysilicon layers on the surface of a wafer tends to offer more flexibility in the design of multilayered structures than simply etching into the wafer itself [3]. However, the process by which polysilicon is deposited on a wafer is slow by nature and thus generally only used to produce thin films [66]. Also, the films it produces have inherent stress gradients throughout their thickness, such that they tend to require additional processing to avoid the curling of any polysilicon structures that are released from the wafer [11].

A structure made of bulk-machined single-crystal silicon (SCS) does not need such additional processing [13]. Also, thicker comb teeth can be made from layers of SCS, which can

increase the vertical distance between the centerlines of the fixed and movable teeth. With a greater offset between the centres of the opposing combs, larger displacements can be achieved by the movable combs. Thicker micromirror structures are also more likely to stay flat during high speed scanning, and the pre-polished surfaces of SCS wafers are very smooth and flat – which makes them suitable to become components of optical devices [11, 13, 19, 22].

Finally, different components of a comb drive can be electrically isolated relatively easily from each other if they are machined out of polysilicon layers on top of a wafer – simply by etching through the layers in the areas around the components to be isolated. However, the same thing can be done with an SCS device layer of a silicon-on-insulator (SOI) wafer, which is a thin wafer bonded to a regular-thickness wafer (called a handle wafer), with an insulating silicon dioxide layer in between them.

### ***3.1.2 Allowable Design Versatility***

Depending on the masks used and the subsequent horizontal patterns etched into the wafers, many fabrication processes can produce comb drives capable of not only vertical actuation but also tilting and horizontal movement. Generally, this multi-functionality has to do with how many electrically separate fixed combs can be produced in the comb drive, and where they can be placed relative to the movable portion of the comb drive, as shown in figure 3.1. The fixed combs will pull the movable combs in the direction in which they are offset from them. Some processes can produce fixed combs both above and below the movable combs, for instance, thus enabling electrostatic forces to act on the movable combs in both vertical directions. Separate fixed combs on either side of the movable portion of a comb drive can alternately pull on one side of it at a time. Often this is used to tilt a micromirror that is steering a beam of light.

### ***3.1.3 Trimming of Springs and Teeth***

Fabrication processes for vertical comb drives that allow the trimming of the thickness of their springs separate from that of their comb teeth, and/or the adjustment of the vertical overlap between their opposing comb teeth, are more versatile in the types of vertical comb drives they can produce. They also tend to be more complex than other fabrication processes.

The thickness of the springs in a comb drive is related to the stiffness of the springs – which determines the rate of increase of the restoring force they apply on the movable combs as

they displace. Generally this parameter is meant to be minimized so that the displacement of the movable combs can be maximized. However, the restoring forces provided by the springs in other directions, also influenced by their thickness, are usually meant to be maximized in order to reduce accidental displacement of the movable combs in those directions – which can lead to electrical discharging between them and the fixed combs. Being able to change the thickness of the springs, as opposed to just their width and length (without affecting the other dimensions of the comb drives), allows for optimization of the compliance of the springs in different directions.

The initial vertical overlap between the fixed and movable comb teeth is one of the characteristics that determine the electromechanical response of the comb drives [7]. If the comb drives are being used as actuators, the initial vertical overlap is related to the initial vertical force applied to the movable combs by the voltage difference between the opposing combs (which can be important for micropositioning, if not resonating applications). Similarly, if the comb drives are being used as sensors, the initial vertical overlap between the fixed and movable combs is related to the initial capacitance of the comb drive, and the initial capacitance change it undergoes as a mechanical force is applied to its movable combs. Using a fabrication process that allows the amount of overlap to be adjusted (for example, with timed etches) allows a designer to further optimize the performance of her comb drives.

### ***3.1.4 Horizontal Alignment between Fixed and Movable Combs***

Properly aligning the movable comb teeth in a comb drive between the fixed comb teeth in the horizontal direction is especially important for a comb drive that is to be used as an actuator, in order to prevent displacement in unintended directions and even shorting between the fixed and movable combs. The voltage difference between the fixed and movable combs attracts the movable combs towards the fixed combs. In addition to the component of the electrostatic force that acts parallel to the sides of each movable tooth, pulling it in the vertical direction, a component of the electrostatic force also acts perpendicular to those sides, pulling the movable tooth horizontally towards its adjacent fixed teeth. Ideally, this force will be balanced by its counterpart on the other side of the tooth pulling it in the opposite direction. These horizontal forces will only be equal, however, if the gaps between the fixed and movable teeth on both sides of the teeth are equal.

## 3.2 Comparison of Fabrication Processes

Table 3.1 compares the fabrication processes discussed in this chapter in terms of the characteristics described in the sections above. As can be seen in the table, most of the fabrication processes position their movable teeth between their fixed teeth by patterning both of their horizontal dimensions with one mask. Most of the processes etch their combs and springs from SCS layers, while a few etch theirs from polysilicon layers. Some processes etch both sets of their combs in the same silicon layer, and then create the vertical offset between them by etching the tops of their bottom teeth down and the bottoms of their top teeth up, which allows for some control over the amount of overlap between the teeth. If space is left beneath the bottom teeth, usually bi-directional vertical actuation can be achieved by patterning the fixed and movable combs such that some of them are the bottom teeth and some of them are the top teeth. Horizontal actuation can also be achieved by not etching away the tops and bottoms of some of the comb pairs. Other processes etch their opposing combs from silicon layers on opposite sides of a planar insulator layer (ie. the upper combs are etched from the top silicon layer and the lower combs are etched from the bottom silicon layer). Having such an insulator layer between the combs automatically electrically isolates them from each other, but makes it impossible for them to have an initial overlap. Again, if space is left beneath the lower conductive layer, and at least one of the conductive layers can be etched through to the insulator layer around separate electrodes, the fabrication process has the potential to create comb drives capable of bi-directional vertical, horizontal, and tilting motions – if the movable portions of the comb drives include both conductive layers. Finally, for simplicity, while many processes etch the spring beams in the same steps as some of the comb teeth (so that they are the same thickness as the teeth), with an extra photolithography step most of these processes could, theoretically, be modified to allow for further trimming of the spring beams.

What follows are brief descriptions of the fabrication processes listed in table 3.1. This is to give the reader an idea of what sort of equipment and fabrication techniques they involve.

### 3.2.1 *Displaced Anchor Processes*

This section describes three fabrication processes for vertical comb drives that etch their springs and combs entirely from the device layer of an SOI wafer. The springs and combs retain the full thickness of the layer while it is etched through around them. After the insulating layer

is etched away from beneath one set of combs their anchoring points to the rest of the wafer are displaced vertically, and various methods are employed to make the displacement permanent.

All three processes generally involve the patterning of the front of an SOI wafer with a single mask, outlining the combs, the springs, and the rest of their associated electrodes. These outlines are then deep-reactive ion-etched (DRIEed – an etching technique that produces high aspect ratio trenches) through the device layer of the SOI wafer, and parts of the buried insulator layer are etched away such that the movable combs and springs (and anything else that will be displaced to create the vertical offset between the movable combs and the fixed combs) are released from the handle wafer.

The first process [14] also etches away the parts of the handle wafer that lie beneath the areas of the device layer that will be displaced. It also etches extra holes through the device layer along with the outlines of the combs so that another silicon wafer, that has been DRIEed to have matching pillars, can be positioned on top of the SOI wafer. Some of these pillars line up with what will be the lower combs, and push them down. Annealing is done to relieve the stresses in the comb anchors, causing permanent plastic deformation, before the top wafer is removed.

The second process [6] grows, patterns, and etches through a layer of silicon dioxide on top of the device layer before it is patterned with the outlines of the combs and springs. The oxide is protected by a layer of polysilicon while the device layer and buried insulator layer are etched through. Once the structures that are covered with oxide are released from the handle wafer they bow upwards to relieve the compressive stress in the oxide (that comes from the thermal mismatch between the oxide and the SCS). Suspension bars at the ends of these bridges rotate to allow them to create shallow arches, and the set of combs that is suspended between a pair of these bridges is lifted upwards.

Finally, the third process [67] involves etching the outlines of “stiction pads” that are attached to one set of combs at the same time as the combs. After the buried insulator layer beneath the stiction pads is etched away in a solution of hydrofluoric acid, the wafer is dried in such a way as to allow the surface tension of the shrinking rinse water droplets to pull the stiction pads down to the surface of the handle wafer. The bond between the two SCS layers can then be enhanced with annealing.

### ***3.2.2 Single Wafer Processes***

This section describes three fabrication processes for vertical comb drives that etch their springs and combs entirely from a single SCS wafer. All of the processes have the ability to adjust the vertical overlap between their opposing comb teeth by etching the tops of their bottom teeth and the bottoms of their top teeth to whatever depth and height the designer chooses. Also, they have the potential to offer a couple of options as to the thickness of their springs. Their springs can be the same thickness as some of their combs, or, with carefully-timed etches, the tops and bottoms of their spring beams can be etched at the same time as the tops and bottoms of the comb teeth, such that the thickness of the spring beams is equal to the amount of overlap between the teeth, as shown in figure 3.2.

#### ***3.2.2.1 (111) Single Wafer Process***

The (111) single wafer process [23] is performed on an SCS wafer of (111) orientation. Two masking layers are deposited and patterned – the first layer defines the horizontal gap between the fixed and movable teeth, the second generally covers the areas of the wafer the upper structures will be fabricated from. Ultimately, the areas of the wafer that are covered by both masking layers will become the upper structures, the areas covered by only the first masking layer will become the lower structures, and the areas that are uncovered will become the spaces etched between the structures, as shown in figure 3.3. The areas covered by only the second masking layer, extending a little ways over the sides of what will be the upper teeth, will form steps in the trenches to be etched into the wafer that allow the undercut beneath the upper structures to be higher than that of the lower structures.

After the formation of the masking layers, the wafer is DRIEed into (which also thins the exposed areas of the first masking layer). The second masking layer is stripped, and the wafer is DRIEed again so that trenches with two different depths are formed between the comb teeth. The sidewalls of the trenches are passivated with an etch-stop film, and the wafer is DRIEed further to expose the sidewalls to be etched. The structures are then released with a wet lateral etch that follows the crystal planes in the (111) wafer to give the teeth square bottoms, undercutting the teeth at the height prescribed by their passivated sidewalls. Finally, the thinned parts of the first masking layer are etched through, the tops of the lower structures are DRIEed down to set the initial vertical offset or overlap between the fixed and movable combs, and the rest of the masking and passivating layers are stripped.

Additional processing is required to electrically isolate the fixed and movable combs from each other. An example method involves creating separate polysilicon shells over the teeth to form conducting layers capable of holding different electrical potentials [23]. In this method, all of the exposed silicon on the wafer is thermally oxidized, the polysilicon is deposited, and a masking layer of metal is deposited that does not reach the bottoms of the trenches in the wafer. The exposed polysilicon at the bottoms of the trenches is etched through to isolate the shells over the different sets of combs.

#### **3.2.2.2 (100) Single Wafer Process**

The (100) single wafer process [10] is very similar to the (111) one. It is performed on a (100) SCS wafer, however, and the etch that releases the movable structures on the wafer is isotropic. Hence the height the bottoms of the upper structures are undercut to does not depend on the crystal planes in the wafer at all, but the depth of the passivated sidewalls of the structures and the amount of time the undersides of the structures are exposed to the etchant. The opposing combs produced by this process are likely able to be electrically isolated from each other with additional process steps similar to those used with the (111) process.

#### **3.2.2.3 BELST II Process**

The boron etch-stop assisted lateral silicon etching (BELST) II process [7] is also performed on a (111) SCS wafer, specifically an *n*-type wafer. An arrangement of masking layers is built on the wafer's top surface similar to that of the above-mentioned processes – such that the areas of the wafer left uncovered will become the spaces in between the structures, the areas with the maximum number of masking layers will become the upper structures, and the areas with fewer masking layers will become the lower structures.

A further masking layer is used to pattern holes that are subsequently DRIEed into the wafer to hollow-out what will become the boron etch-stop posts that anchor the fixed combs and ends of the springs to the wafer. That masking layer is then stripped, and the wafer is DRIEed again to create trenches of two different depths, so that there are deeper trenches inside the posts than there are beside what will be the springs and teeth. Boron is then diffused into the sidewalls of the trenches, and the masking layers are thinned to uncover the structures to be lowered. The tops of those structures are DRIEed down to set the initial vertical offset or overlap between the fixed and movable combs, and create the trenches the lateral etch is to begin from. The movable structures are then released with a wet lateral etch that follows the crystal planes in the (111)

wafer, undercutting the upper teeth and springs at the height prescribed by their  $p$ -doped sidewalls. The etch stops at the similarly-doped walls of the anchors for the springs and fixed teeth. Finally, the rest of the masking layers are removed.

Because the BELST II process uses oppositely-doped sidewalls as an etch-stop for the undercut of the mechanical structures, it does not require that additional process steps be appended to it to electrically isolate its opposing combs from each other, as it automatically creates  $p$ - $n$ - $p$  junctions between them.

### ***3.2.3 Polysilicon Trench Re-Fill Processes***

Depositing polysilicon over a wafer that has had narrow trenches etched into it can produce continuous polysilicon structures of varying thicknesses. These can include thin structures such as springs that are made from the polysilicon that was deposited over the flat areas of the wafer, and thick structures such as comb teeth that are made from the polysilicon that has filled the trenches. Also, rigid polysilicon micromirrors can be made that are periodically re-inforced by the thicker polysilicon.

Generally, polysilicon trench re-fill processes begin by depositing, patterning, and etching two masking layers on the front of a silicon wafer. DRIEing into the wafer, stripping the top masking layer, and DRIEing into the wafer again produces trenches of two different depths. The bottom masking layer is then stripped, and a layer of silicon dioxide is grown on the wafer. A layer of polysilicon is deposited on the front of the wafer, filling the trenches to become the thick parts of the structure the comb teeth will be etched from. The polysilicon layer is patterned and etched through to separate the electrodes and define the shapes of the springs. With another masking layer, the polysilicon in some of the trenches can be etched down to further adjust the offset between opposing teeth.

Three methods by which to clear away regions of the wafer beneath the polysilicon combs and release the movable combs and springs from the wafer have been suggested in the literature. The first method [24] involves simply depositing and patterning a layer of photoresist on the back of the wafer, and subsequently DRIEing through the wafer beneath the combs and springs. The oxide that lined the trenches is removed in a hydrofluoric acid solution, releasing the movable combs and springs from the wafer. The portion of the wafer beneath the area between

different banks of movable combs can be left as a large mass if the comb drive is to be used as an accelerometer.

The second method [12] involves depositing a layer of silicon nitride on the front of the wafer to protect the exposed areas of the polysilicon layer. The masking layers on top of the wafer are then etched through in a few key areas so that the regions of the wafer beneath them can be exposed to a tetramethylammonium hydroxide solution. This etches away the wafer below the polysilicon combs and springs while the oxide layer that lined the trenches protects them from below. The combs and springs are released from the wafer by etching away the oxide and nitride that is encasing them with hydrofluoric acid.

Finally, the third method [11] requires the silicon wafer to be of a (111) orientation. This process begins with three masking layers and three DRIEs to create trenches of three different depths on the front of the wafer. The oxide that lines the side walls of the deepest trenches will act as an etch-stop layer during the etching of the silicon wafer beneath the polysilicon combs and springs. Again, silicon nitride is deposited over the polysilicon layer to protect it, and it and the oxide layer is etched through in a few key areas around the combs and springs. Through these holes the wafer is DRIEed to set the depth of the space that will be beneath the combs and springs, and to expose the non-(111) crystal planes on the trench side walls. The wafer is immersed in a potassium hydroxide solution that etches the silicon laterally while the oxide and nitride layers protect the polysilicon, and the oxide in the deep trenches defines the borders of the etch beyond the comb structures. The combs and springs are released from the wafer by etching away the oxide and nitride that is encasing them with hydrofluoric and phosphoric acid. The passivated side walls can also be used to leave part of the SCS wafer beneath a mirror structure to enhance its rigidity.

### ***3.2.3.1 Polysilicon Trench Re-Fill Process with an Upper Etch-Stop Layer***

Including the creation of an upper etch-stop layer in the process allows the fixed teeth of the vertical comb drive to be made from the SCS wafer. This process [1] uses a *p*-type (100) silicon wafer, and begins with creating an upper etch-stop layer in the wafer by deep boron diffusion, using thermally-grown silicon dioxide as a masking layer. The thickness of the etch-stop layer defines the thickness of the fixed teeth that will be etched from it. Trenches of a single depth are dry-etched through the etch-stop layer and into the silicon beneath it, using an electroplated nickel masking layer. The nickel is stripped, and a low-pressure chemical vapour

deposition (LPCVD) silicon dioxide is deposited to isolate the polysilicon layer from the silicon wafer. An LPCVD polysilicon layer is deposited, filling the trenches so that thick movable comb teeth as well as thin springs can be etched from that layer. The polysilicon layer is patterned and etched to form the movable combs and springs, and the polysilicon in some of the trenches is etched further to lower the tops of some of the movable teeth. Another LPCVD silicon dioxide layer is deposited over the polysilicon to protect it during the etching of the wafer below it; the oxide is patterned and etched through to expose some of the areas of the wafer that have not had extra boron implanted in them. Ethylenediamine pyrocatechol is used to undercut these areas to create space beneath the combs and springs, while the polysilicon movable combs and springs are protected by the oxide layers above and below them, and the fixed combs are protected by their high dopant level. Finally, the movable structures are released by etching away the oxide that is encasing them with buffered hydrofluoric acid.

### ***3.2.4 Custom SOI Wafer Processes***

This section describes five fabrication processes for vertical comb drives that begin by fabricating their own SOI or double SOI wafers (double SOI wafers have two device layers separated from each other and the handle wafer by two insulator layers). Generally these processes add a silicon layer after the one below it has been patterned and etched to provide space beneath what will be the movable combs and springs. The “over-sized fixed teeth” left behind in the lower layer will be narrowed later on in the processes when the movable teeth above them are patterned and etched. Because the fixed and movable combs in these processes are etched from different layers in a stack of planar silicon layers, none of the processes are able to adjust the initial vertical overlap between their opposing combs. Their opposing combs are generally automatically electrically isolated from each other, however, by being etched from separate silicon layers.

The basic custom SOI wafer process [4] begins by patterning and DRIEing the outlines of over-sized fixed comb teeth into the front of a silicon wafer that will become the handle wafer of the SOI wafer. A layer of silicon dioxide is thermally grown on this wafer and another wafer that will become the device layer. The two wafers are then bonded together, the top wafer is polished down to the required thickness of the device layer, and the final outlines of both sets of comb teeth are patterned on its surface, aligned over the trenches in the handle wafer. The

device layer is DRIEd through, the oxide above the over-sized areas of the fixed teeth is removed, and the handle wafer is DRIEd to trim the fixed teeth to their final shape. Finally, the rest of the exposed oxide is removed.

#### ***3.2.4.1 Custom Double SOI Wafer Process***

The custom double SOI wafer process [17, 68] is similar to the custom SOI wafer process, except it begins by patterning and DRIEng the outlines of the over-sized fixed comb teeth through the device layer of a standard SOI wafer. Silicon dioxide is then grown on a separate silicon wafer, and that wafer is fusion-bonded on top of the etched device layer. The silicon wafer is ground and polished down to the desired thickness of the movable combs and springs, and then patterned and DRIEd through with their outlines, as well as the outlines of the fixed combs. The exposed parts of the oxide beneath the top silicon layer are etched through, and the pattern is continued through the bottom device layer to narrow the fixed teeth to their final width.

Because separate banks of fixed combs can be created in the lower device layer, tilting of the movable combs can be achieved with this process.

#### ***3.2.4.2 Bulk Oxidation Process***

The bulk oxidation process [3] is similar to the custom double SOI wafer process in that it etches the outlines of over-sized fixed comb teeth through the device layer of an SOI wafer before stacking another silicon layer on top of it that the movable combs and springs will be etched from. In this process, however, the extra silicon layer is deposited polysilicon, and the spaces etched through the device layer are subsequently filled with silicon dioxide so that the polysilicon can be deposited over a planar surface.

The process begins with the formation of a sacrificial silicon dioxide block in the device layer beneath the area where the movable comb teeth will be fabricated. This is done by DRIEng closely-spaced trenches in the device layer, thermally oxidizing the remaining silicon between them, and depositing further oxide to fill the rest of the trenches and form a sacrificial layer on top of the wafer. (In the areas of the device layer to become the fixed combs, the trenches are spaced further apart to leave SCS regions for the fixed teeth to be etched from.) The process continues with the etching of windows through the top oxide to allow the springs to be anchored to the wafer. Silicon nitride is deposited to electrically isolate the surface micromachined structures from the device layer, and polysilicon is deposited to act as the upper structural layer. Finally, the polysilicon over top of the fixed teeth is removed and a masking

layer is prepared to pattern the final outlines of both sets of teeth. The comb teeth are etched, the masking layer is stripped, and all of the sacrificial material is removed to release the movable structures.

#### ***3.2.4.3 Custom Double SOI Process with Thinned Springs***

The springs in the custom double SOI wafer process can be thinned if two masking layers are patterned on the top device layer [69]. The removal of the second masking layer, after the outlines of the springs and combs have been etched, can expose the tops of the springs to etching while the first masking layer continues to protect some of the comb teeth. If the movable teeth are thinned along with the springs, upwards electrostatic forces can be applied on them by full-thickness fixed combs left in the top device layer.

#### ***3.2.4.4 Stacked Device Layer Process***

The stacked device layer process [70] is somewhat similar to the custom double SOI wafer process. However, it does not grow oxide on top of the device layer of the SOI wafer before bonding another silicon wafer to it, and ultimately two silicon wafers are stacked on top of the device layer – the movable comb teeth are etched from the lower one, and the springs are etched from the upper one.

This process begins with patterning and DRIEing the outlines of over-sized fixed comb teeth through the device layer of an SOI wafer. A silicon wafer is bonded on top of the device layer and polished down to the thickness of the movable comb teeth. The top of the new silicon layer is patterned for two DRIEs. The first DRIE goes through the new silicon layer and exposes the areas of the over-sized bottom comb teeth that are to be etched away. The second DRIE etches away those areas to narrow the bottom teeth and align them with the top teeth. It also leaves only supporting structures for the next silicon layer, and the top teeth in the top silicon layer (or rather extra-long top teeth – at this point they are supported by only the inner edges of the bottom combs). The second silicon wafer is bonded on top of the remnants of the first silicon wafer, and polished down to the thickness of the springs. It is also patterned for two DRIEs. The first DRIE goes through the second silicon wafer and removes the ends of the top teeth over the inner edges of the bottom combs. The second DRIE etches the outlines of the springs and the platform connecting the movable teeth through the second silicon wafer.

This fabrication process can be thought of as one that includes extra process steps so that its comb pairs can be hidden beneath a micromirror. Such micromirrors are usually intended for array applications where a high fill-factor is desired.

### ***3.2.5 SOI Wafer Processes***

This section describes seven fabrication processes for vertical comb drives that, for the most part, etch their combs and springs from standard, ready-made SOI or double SOI wafers, or otherwise build these wafers before etching parts of them. Because the fixed and movable combs in these processes are etched from different layers in a stack of silicon layers, none of the processes are able to adjust the initial vertical overlap between their opposing combs. Their opposing combs are automatically electrically isolated from each other, however, by being etched from different silicon layers that are separated by insulating layers.

#### ***3.2.5.1 Double SOI Wafer Process***

The double SOI wafer process [18] begins with a double SOI wafer. Two masking layers (silicon dioxide and photoresist) are deposited and patterned on its top device layer. The photoresist, being the top masking layer, defines the outlines of the combs and springs, and the silicon dioxide covers the regions that will retain the full thickness of both device layers. (That is, after the photoresist has been patterned, the silicon dioxide is etched through again in the areas that are not covered with photoresist, so that there is no need for the precise alignment of the two layers.) The top device layer is then DRIEd through, and the exposed regions of the top buried insulator layer are reactive-ion etched (RIEd) through. The photoresist is stripped, and the outlines of the combs and springs are DRIEd through the bottom device layer while the regions in the top device layer not covered with silicon dioxide (presumably above the movable combs and springs in the bottom device layer) are also etched away. Finally, the movable structures are released from the handle wafer by patterning photoresist on the back of the handle wafer, DRIEng through it, and then RIEing through the bottom insulator layer.

A variation on this process [19] uses a double SOI wafer that has its two device layers made from polysilicon.

#### ***3.2.5.2 Doubled SOI Process***

The doubled SOI process [9, 71] begins by building a double SOI wafer, by depositing a layer of silicon nitride on top of the device layer of a standard SOI wafer to form a second

insulating layer, and a layer of polysilicon on top of the nitride to form a second device layer. This process also etches through the handle wafer and the subsequently exposed bottom insulator layer from the back of the wafer beneath the movable structures to release them. However, it patterns only a single masking layer on the top device layer. Hence while the outline of the combs and springs are etched through the polysilicon, nitride, and bottom SCS device layer, nothing is done to remove the excess polysilicon above the lower comb teeth or the SCS device layer below the upper comb teeth.

### ***3.2.5.3 Epipoly Layer Process***

The Epipoly layer process [8], like the doubled SOI process, deposits another insulating layer and another silicon layer on top of a standard SOI wafer to create a double SOI wafer. It etches its lower comb teeth from the device layer of the original SOI wafer, and etches through the handle wafer and the original insulator layer beneath the movable structures to release them. However, in this process the second device layer that the upper comb teeth are etched from is a thick Epipoly layer – a type of silicon layer that can be deposited relatively quickly and with low internal stress in an epitaxial reactor. Also, the springs in this process are made from a separate polysilicon layer – one that is deposited and etched before the Epipoly layer is deposited.

The process begins with the deposition of an insulator layer on top of the device layer of an SOI wafer. The insulator layer is patterned and etched through to create anchor sites for the springs. A polysilicon layer is then deposited, patterned, and etched through to create the spring structures. Another insulator layer is deposited on top of the wafer, as well as an Epipoly layer and a masking layer. The masking layer is patterned with the final outlines of both sets of comb teeth, and the pattern is continued through the Epipoly, top insulator, and original device layers with successive vertical anisotropic etches. Silicon dioxide is then grown on all exposed silicon surfaces to create protective shells over them, and holes are etched through the oxide over the regions of the Epipoly layer to be etched away. Those regions are etched with  $\text{XeF}_2$ , the handle wafer is DRIEd through from the back (below the movable structures), and the exposed insulator layer beneath the structures is etched through to release them.

### ***3.2.5.4 Full SOI Wafer Process***

The full SOI wafer process [22] takes a fairly direct approach to fabricating vertical comb drives from an SOI wafer. It patterns two masking layers on the front of the wafer and two on the back. It performs two DRIEs on the front of the wafer and two on the back, such that with

sequential stripping of the masking layers the upper comb teeth retain the thickness of the device layer and the lower comb teeth retain the thickness of the handle wafer, while the springs are etched from the thinned portions of either the device layer or the handle wafer. The etched structures are then released from each other by removing the portions of the insulator layer lying between them.

#### ***3.2.5.5 Custom Thinned SOI Process***

The custom thinned SOI process [72] is similar to the full SOI wafer process, except that it begins by effectively fabricating its own SOI wafer. The handle wafer of the SOI wafer has trenches etched into the front of it before it is oxidized and bonded to the device layer.

The device layer is then patterned and DRIEed through once to separate the top electrodes from each other, and the handle wafer is thinned by chemical-mechanical polishing. The handle wafer is then patterned and DRIEed through once from the back to separate the bottom electrodes and shape the springs. (The springs are etched from the silicon left beneath the trenches originally etched on the front of the handle wafer, so they can be thinner than the bottom combs, etc..) The etched structures are finally released from each other by removing the portions of the insulator layer lying between them.

#### ***3.2.5.6 Thinned Handle Wafer Process***

The thinned handle wafer process [5] etches its upper comb teeth from the device layer of a standard SOI wafer and its lower comb teeth from thinned portions of the handle wafer. The etch that separates the electrodes in the device layer is continued through the thinned portions of the handle wafer so that the upper and lower teeth are automatically aligned with each other. To assist in the etching of the buried insulator layer at the bottom of high aspect ratio trenches between the upper comb teeth, a delay-masking technique is employed during the etching of the device layer. It exposes areas of the layer to be removed above the lower teeth early – so that they may be partially etched down to effectively widen the trenches.

The process begins with the deposition of four masking layers on an SOI wafer that alternate between silicon dioxide and polysilicon. Two lithography and two etching steps are performed on the masking layers such that: 1) the exposed areas of the device layer will become the spaces in between the comb teeth, etc., where the SOI wafer will be etched through, 2) the areas with the full number of masking layers will become the upper structures etched from the

device layer, and 3) the areas with only a single oxide masking layer will become the lower structures, ultimately being comprised of a thinned portion of the handle wafer.

Once the four masking layers are patterned, and while a layer of photoresist remains above them, the device layer is DRIEd part-way through. The photoresist is then stripped, and the exposed areas of the first oxide masking layer are removed (ie., above what will be the lower structures). The device layer is then DRIEd again so that the bottoms of the first set of trenches reach the buried insulator layer. The exposed portions of the insulator layer are then etched through. The masking layers on the back of the wafer are removed beneath where the combs and springs will be etched, and the exposed areas of the handle wafer are DRIEd from the back until they are the same thickness as the device layer. Finally, the movable structures are released with a DRIE through the wafer from the front (which also removes the rest of the unwanted portions of the device layer above the lower structures), and any exposed oxide is etched away.

#### ***3.2.5.7 Thinned Handle and Springs Process***

The thinned handle and springs process [16] also etches its upper and lower comb teeth from the device layer and the handle wafer, respectively, of a standard SOI wafer. It begins by patterning three masking layers on the device layer. With three successive DRIEs and the sequential stripping of the masking layers (and an etch through the buried insulator layer) trenches of three different depths are formed on the front of the wafer. The shallowest trenches stop part-way through the device layer, thinning the portions of the wafer the springs will be etched from. The second shallowest trenches stop on the buried insulator layer, removing the silicon in the device layer above the areas of the handle wafer the lower combs will be etched from. The deepest trenches go through the buried insulator layer and into the handle wafer, defining the outlines of the combs and springs.

The back of the SOI wafer is ground and chemically-mechanically polished to thin the handle wafer. Three masking layers are patterned, and the handle is DRIEd from the back while they are successively stripped. Again, this further thins the portions of the wafer the springs are etched from, and removes the silicon in the handle wafer below the areas of the device layer the upper combs are etched from. It also removes the silicon in the handle wafer beneath the lower combs. Some of the trenches on the back of the wafer also meet the deepest trenches etched from the front, which releases the movable structures.

### **3.2.6 Single Device Layer Processes**

This section describes three fabrication processes for vertical comb drives that etch their combs and springs from a single layer on top of a handle wafer. The vertical offset between their opposing combs comes from etching the tops of their bottom teeth down, if not also the bottoms of their top teeth up. The processes that etch their teeth from both directions also have the potential to offer a couple of options as to the thickness of their springs. As shown in figure 3.2, their springs can be the same thickness as some of their combs, or, with carefully-timed etches, the tops and bottoms of their spring beams can be etched at the same time as the comb teeth so that their thickness is defined by the amount of overlap left between the teeth.

#### **3.2.6.1 Simple SOI Process**

The simple SOI process [73-75] begins by depositing and patterning two masking layers on top of the device layer of a standard SOI wafer. The bottom masking layer is etched through twice. The first time is before the top masking layer is deposited, so that spaces can be left that only the top masking layer will cover (such as the bottom comb teeth and the springs). The second time it is etched is after the top masking layer has been etched through with the final outlines of the combs and springs – this pattern is then continued through the bottom masking layer, so that there is no need for precise alignment between the layers.

Once the masking layers are defined, the device layer of the SOI wafer is plasma-etched partially through with the outlines of the combs and springs, the top masking layer is stripped, and the device layer is etched again to finish separating the electrodes and to lower the tops of the bottom teeth and springs (that is, the vertical offset between the combs is directly related to the thickness of the bottom comb teeth). Finally, the movable structures in the device layer are released from the handle wafer by etching away the buried insulator layer beneath them.

#### **3.2.6.2 Custom SCS Layer Process**

The custom SCS layer process [76, 77] begins by patterning and DRIEing the back of an SCS wafer twice – once to create space beneath all of the combs and springs that will be etched from the wafer, and once to raise the bottoms of the upper teeth above those of the lower teeth. The back of the SCS wafer is then anodically bonded to a glass wafer, and the SCS wafer is thinned by etching down its top in potassium hydroxide. Finally, the outlines of the combs, springs, and the rest of the electrodes are DRIEed through the SCS wafer from the front. The

tops of the lower comb teeth can also be etched down to increase the vertical offset between them and the upper teeth [77].

### ***3.2.6.3 Partially-Exposed Photoresist Process***

The partially-exposed photoresist process [21] begins with a glass substrate that has a patterned layer of titanium on top of it. A thick layer of photoresist is spin-coated on top of the titanium. The photoresist will act as the structural layer from which the combs and springs are made. The photoresist is partially exposed to ultraviolet light (that is, not exposed all the way through) from the top to define the regions of the photoresist that will be removed above the lower combs. The photoresist is then partially-exposed from the bottom through the areas of the glass substrate not obscured with titanium. This defines the regions of the photoresist that will be removed beneath the upper combs. Finally the photoresist is exposed from the top again, this time all the way through, defining the shapes of the combs and springs.

The photoresist is developed to remove the portions of it that have been exposed, and copper is sputtered on the photoresist from the front to create conducting shells on the tops and sides of the photoresist structures. To keep the copper layer from being continuous over all of the structures, the pillars anchoring the upper structures to the glass substrate are designed with an overhang, the bottom of which does not get covered in copper.

### ***3.2.7 Multiple Wafer Processes***

Finally, this section describes two more fabrication processes for vertical comb drives that etch their opposing combs from different substrates, before aligning and bonding the separate structures together.

#### ***3.2.7.1 Flipped Chip Process***

The flipped chip process [78] fabricates its movable combs, springs, and half of a supporting frame from a standard SCS wafer. Its fixed combs and the other half of the supporting frame are made from a standard SCS wafer bonded to a glass wafer. A flip chip aligner bonder is used to align the wafers and bring them into contact with each other. The optical arrangement inside the equipment allows both sides to be bonded to be seen at once so that coarse alignment can be achieved; 4 alignment keys fabricated on the wafers guide them into their final positions as they are brought together. The two halves of the supporting frame are then pressed together and the structures are heated to create eutectic bonds between metal

coatings. The thickness of the supporting frame determines the initial vertical overlap between the opposing comb teeth.

A variation [15] on the process uses an SOI wafer rather than simply a silicon wafer as the top substrate. The movable combs and springs are machined from one side of the SOI wafer while another set of fixed combs are machined from the other side. When the SOI wafer is bonded to the other silicon wafer, the movable combs end up having fixed combs both above and below them.

### ***3.2.7.2 Parts-Transfer Process***

The parts-transfer process [13] molds a polydimethylsiloxane (PDMS) substrate using a silicon wafer that has been etched such that it produces raised structures on the PDMS that will set the vertical offset between the upper and lower combs of the comb drive. The device layer of an SOI wafer is then etched through with the outlines of what will become the lower, fixed electrodes, and the buried oxide layer beneath the structures to be transferred is etched away until there is only a narrow pillar of the oxide left still holding them to the handle wafer. The top of the SOI wafer is aligned with and then pressed against the PDMS substrate, breaking the oxide pillars and leaving the electrode structures from the device layer stuck to the PDMS. This procedure is repeated with another SOI wafer that has had the outlines of what will be the movable combs and springs etched through its device layer. The anchors of the springs are pressed against the raised areas of the PDMS.

## **3.3 Summary and Recommendations**

Table 3.1 is intended to assist researchers in finding the fabrication processes that will produce the types of vertical comb drives they require for their particular applications. The descriptions of the processes are intended to give researchers an idea of what equipment and fabrication techniques are involved in carrying them out.

Most of the fabrication processes etch their combs and springs from silicon – sometimes polysilicon, but usually single-crystal silicon, which tends to allow for taller comb teeth. Most of the processes also position their opposing teeth precisely between one another by patterning all of their combs with the same mask.

With the clever design of the masks for the fabrication process, many processes can produce comb drives capable of not only vertical actuation in both the upwards and downwards

directions, but also tilting motions and even horizontal actuation. This multi-functionality is determined by how many separate fixed combs can be produced in the comb drive, and where they are relative to the movable portion of the comb drive. Some processes can produce fixed combs both above and below the movable combs, for instance, enabling electrostatic forces to act on the movable combs in both vertical directions. A common arrangement of fixed combs that are vertically offset from the movable combs has them electrically separate in the horizontal direction and positioned on either side of the movable combs so that the movable combs can be tilted as voltages are applied to the fixed combs on one side at a time.

Some of the fabrication processes are able to control the initial vertical overlap between their fixed and movable teeth, and some are able to control the thickness of their springs independently of that of the other structures in the comb drive. For simplicity, many processes etch their spring beams in the same steps as their comb teeth (so that they are the same thickness as some of the teeth), but with an extra photolithography step most of these processes could, theoretically, be modified to allow for further trimming of their spring beams. Of course, versatility in a process tends to lead to complexity.

Some processes etch both sets of their combs in the same silicon layer, and then create the vertical offset between them by etching the tops of their bottom teeth down and the bottoms of their top teeth up, which allows for some control over the amount of overlap between the teeth. If space is left beneath the bottom teeth, usually bi-directional vertical actuation can be achieved by patterning the fixed and movable combs such that some of them are the bottom teeth and some of them are the top teeth (horizontal actuation can also be achieved by not etching away the tops and bottoms of some of the comb pairs). Other processes etch their opposing combs from silicon layers on opposite sides of a planar insulator layer (that is, the upper combs are etched from the top silicon layer and the lower combs are etched from the bottom silicon layer). Having such an insulator layer between the combs automatically electrically isolates them from each other, but makes it impossible for them to have an initial overlap. In this case, if space is left beneath the lower conductive layer, and at least one of the conductive layers can be etched through to the insulator layer around separate electrodes, the fabrication process has the potential to create comb drives capable of bi-directional vertical, horizontal, and tilting motions – if the movable portions of the comb drives include both conductive layers.

It seems that the simplest fabrication process for vertical comb drives is the simple SOI process [73-75]. It creates the comb drives in the device layer of a standard SOI wafer, etching the tops of the lower teeth down to generate the vertical offset between them and the upper teeth (that retain the full thickness of the device layer). With the clever design of the masks used in the process, comb drive actuators capable of electrostatically drawing their movable combs in the full range of directions shown in table 3.1 should be able to be produced.

If it is necessary to change the thickness of the springs relative to that of the combs, it is expected that another mask and subsequent patterning and etching steps could be added to the process. Since the amount of initial vertical overlap between the teeth is not independent of the thickness of the shorter teeth, to more completely control the amount of overlap between the teeth, process steps that will vary the relative heights of the bottoms of the comb teeth must be added. These could include etching the bottom of the device layer before it is bonded to the oxidized handle wafer, as in the custom SCS layer process [76, 77].

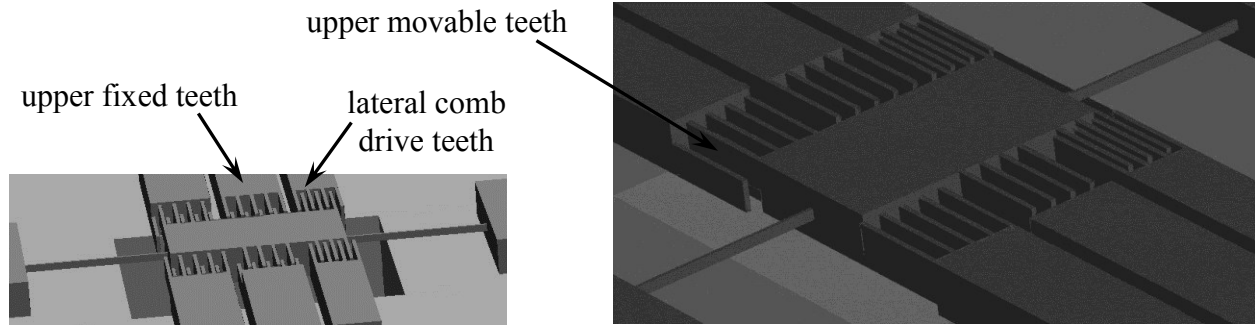


Figure 3.1: Schematics of a multi-functional vertical comb drive, made using a process very similar to the custom SCS layer process [77]. The movable part of the comb drive can be made to tilt back and forth because the fixed combs on either side of the springs are separate from each other. The movable part of the comb drive can also be electrostatically pulled both upwards and downwards because some of the movable combs are the upper combs and some of them are the lower combs. Also, some of the movable combs have no vertical offset from their opposing fixed combs, so when a voltage difference is applied to them they can cause the comb drive to move horizontally.

Table 3.1: A comparison of fabrication processes for vertical comb drives.

Fabrication Process	Allowable Design Versatility (Potential Directions of Actuation)	Vertical Offset Mechanism	Electrical Isolation between Combs	Alignment Mechanism for Opposing Comb Teeth	Structural Materials		Allowable Design Adjustments	
					Springs	Teeth	Spring Thickness	Tooth Overlap
<b>displaced anchor</b> (Sasaki 2004, Kim 2000, Kim 2006)	↕ vertical offset in 1 direction, fixed combs can be separated in horizontal direction	anchors of one set of combs are displaced vertically	electrodes etched from separate parts of device layer on SOI wafer	opposing teeth originally etched in same plane			no	
<b>(111) single wafer</b> (Kim 2002)	↖↗ vertical offset possible in both directions, no offset possible, fixed combs can be separated in horizontal direction	tops of bottom teeth & bottoms of top teeth are etched away	separate conducting shells over structures		SCS		partially	yes
<b>(100) single wafer</b> (Zhang 2005)	↖↗							
<b>BELST II</b> (Tsai 2004)	↖↗							
<b>polysilicon trench re-fill</b> (Wu, 2005 & 2006, Chan 2009)	↑	trenches to be re-filled are etched to different depths, tops of bottom teeth are etched down	p-n-p junction between opposing combs		poly-Si		yes	
<b>polysilicon trench re-fill with an upper etch-stop layer</b> (Srivakumar 2003)	↑		electrodes etched from separate parts of conductive layer		poly-Si & SCS			
<b>custom SOI wafer</b> (Kishimoto 2003)	↕		insulator layer between electrodes	single mask patterns final outlines of all combs				
<b>custom double SOI wafer</b> (Lee 2004, Kumar 2008)	↕	upper & lower teeth machined on separate layers			SCS		no	
<b>bulk oxidation</b> (Yeh 1999)	↖↗	vertical offset in 1 direction, no offset possible, fixed combs can be separated in horizontal direction	insulator between layers of electrodes; electrodes etched from separate parts of layers		poly-Si & SCS			no
<b>custom double SOI with thinned springs</b> (Carr 2006)	↖↗	vertical offset possible in both directions, no offset possible, fixed combs can be separated in horizontal direction						
<b>stacked device layer</b> (Wada 2002)	↕	vertical offset in 1 direction, fixed combs can be separated in horizontal direction	electrodes etched from separate parts of device layer on SOI wafer		SCS		yes	

Table 3.1: Continued.

Fabrication Process	Allowable Design Versatility <i>(Potential Directions of Actuation)</i>	Vertical Offset Mechanism	Electrical Isolation between Combs	Alignment Mechanism for Opposing Comb Teeth	Structural Materials		Allowable Design Adjustments			
					Springs	Teeth	Spring Thickness	Tooth Overlap		
<b>double SOI wafer</b> <i>(Kumar 2009)</i>	 vertical offset possible in both directions, no offset possible, fixed combs can be separated in horizontal direction	upper & lower teeth machined on separate layers	insulator between layers of electrodes; electrodes etched from separate parts of layers	single mask patterns final outlines of all combs	SCS	SCS	no			
<b>doubled SOI</b> <i>(Lim 2005, Teou 2005)</i>							poly-Si, Si <sub>3</sub> N <sub>4</sub> , & SCS		no	
<b>Epipoly layer</b> <i>(Carlen 2005)</i>						Epipoly & SCS				
<b>full SOI wafer</b> <i>(Kozuma 2005)</i>					typical alignment procedure between front- & back-side masking layers	SCS			yes	
<b>custom thinned SOI</b> <i>(Cho 2007)</i>										no
<b>thinned handle wafer</b> <i>(Hak 2004)</i>										
<b>thinned handle &amp; springs</b> <i>(Kim 2009)</i>							SCS & SiO <sub>2</sub>		yes	
<b>simple SOI</b> <i>(Tsuchiya 2004, Hamaguchi 2007, Zickler 2007)</i>			tops of bottom teeth are etched down	electrodes etched from separate parts of device layer on SOI wafer	single mask patterns final outlines of all combs				no	
<b>custom SCS layer</b> <i>(Yang 2005, Liu 2006)</i>			tops of bottom teeth & bottoms of top teeth are etched away	electrodes etched from separate parts of conductive layer						
<b>partially-exposed photoresist</b> <i>(Chang 2008)</i>				separate conducting shells over structures			photoresist & Cu		partially	
<b>flipped chip</b> <i>(Lee 2002, Ko 2006)</i>	 vertical offset possible in both directions, no offset possible, fixed combs can be separated in horizontal direction	upper & lower teeth machined on separate wafers	electrodes etched from separate parts of conductive layer	use of flip chip aligner bonder & alignment keys on wafers				yes		
<b>parts-transfer</b> <i>(Iwase 2008)</i>	 vertical offset in 1 direction, fixed combs can be separated in horizontal direction	substrate molded to set heights of areas combs are fixed to	electrodes placed separately on insulating substrate	alignment of opposing substrates	SCS		yes			

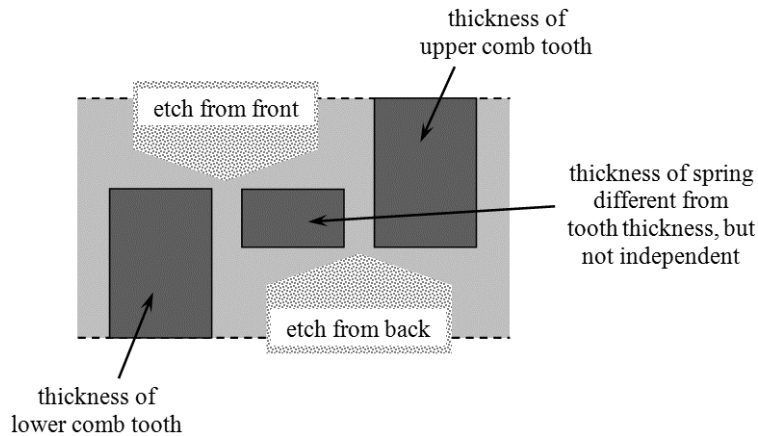


Figure 3.2: Many fabrication processes for vertical comb drives create the vertical offset between the centrelines of their opposing comb teeth by etching the tops of their bottom teeth down and the bottoms of their top teeth up. If these partial etches into the structural layer are shallow enough, they can both be done in the same area, so that the thickness of the springs is equal to the vertical overlap between the comb teeth.

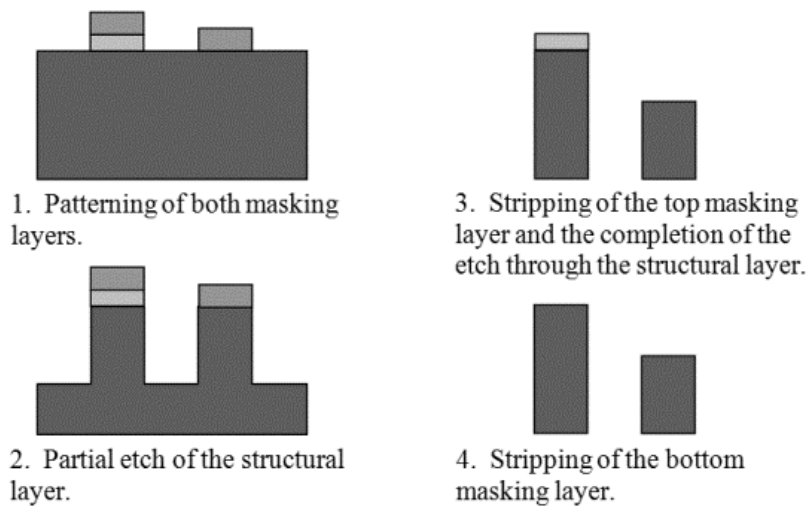


Figure 3.3: A schematic of the cross-section of a structural layer as it undergoes two etches while the masking layers protecting certain regions of it are sequentially removed. In Step 3, the top of what will be the lower structure is etched down as the etch through the structural layer is completed. During this etch the bottom masking layer continues to protect what will be the upper structure.

# Chapter 4 : Fabrication of Vertical Comb Drive Prototypes

The process followed to fabricate the vertical comb drives for the studies detailed in Chapters 5 and 6 is similar to the simple SOI process [73-75] discussed in Chapter 3. A single mask is used to pattern the final outlines of all the combs and spring beams in the device layer of an SOI wafer. The vertical offset between the combs is created by etching down the tops of what become the lower teeth. The handle wafer is etched away from beneath the movable combs and springs, and the movable components are released from the substrate by etching away the buried oxide beneath them. Because the fixed combs can be separated from each other in the device layer, and either the fixed or movable teeth can be the lower teeth, this process can produce fixed combs both above and below the movable combs, as shown in figure 4.1. This will allow electrostatic forces to be applied on the movable combs (and thus a probe that is attached to them) in both the upwards and downwards directions.

The difference between this fabrication process and those previously reported lies in how the upper teeth are masked while the tops of the lower teeth are etched down. A layer of photoresist is spun onto the wafer after the outlines of the combs have been etched through the device layer – such that when the photoresist is removed from the tops of the teeth to be etched down the rest of the teeth remain encased in photoresist so that their sides are protected as well as their tops. This helps prevent the otherwise exposed top corners of the lower teeth from being over-etched, as in figure 4.2. It also allows the etch of the outlines of the combs to get through the device layer without affecting the thickness of the lower teeth, and prevents extra notching [79] of the bottoms of the teeth at the silicon-oxide interface while the lower teeth are etched down.

## 4.1 Fabrication Process Steps

The steps of the process that were followed to fabricate the vertical comb drives are listed below and shown schematically in figure 4.3. They were carried out on an SOI wafer that had a phosphorus-doped device layer that was  $20\pm 0.5\mu\text{m}$  thick and of (100) orientation. The buried oxide beneath the device layer was  $1\mu\text{m}$  thick, and the handle wafer was  $380\mu\text{m}$  thick.

- 1.) The wafer was cleaned in a fresh (110°C-130°C) 3:1 (96%) sulfuric acid and (30%) hydrogen peroxide solution for 15min.
- 2.) Photoresist (HPR 504) was patterned on the front of the wafer, and the device layer was Bosch deep reactive ion etched (DRIEed) through. The bulk of the photoresist was rinsed off with acetone, followed by isopropyl alcohol and then water. The wafer was then cleaned again in the sulfuric acid and hydrogen peroxide solution, which did not need to be freshly made for it to be effective in removing the remaining photoresist. The exposed buried oxide was etched through in an HF solution, so that the contact metals could be deposited on the exposed portion of the handle wafer as well as the device layer.
- 3.) 30nm of chromium and 180nm of gold were sputtered on the front of the wafer and then covered with a thicker photoresist (AZ P4620 – to cover the holes already in the device layer). The photoresist was patterned to define the shapes of the contacts, and the gold was etched through in a solution of potassium iodide and iodine, and the chromium was etched through in a solution of ceric ammonium nitrate and nitric acid. The photoresist was then stripped as before with acetone and the sulfuric acid solution.
- 4.) The outlines of the combs and springs were patterned on the front of the wafer with another layer of photoresist (HPR 506). The device layer was DRIEed through, and the photoresist was stripped with acetone and the sulfuric acid solution.
- 5.) The front of the wafer was again covered in photoresist (two layers of HPR 506), which was patterned to expose the tops of the teeth to be etched down. The teeth were DRIEed until about 8 $\mu$ m remained of the original 20 $\mu$ m, and the photoresist was stripped with acetone and the sulfuric acid solution.
- 6.) A layer of photoresist (HPR 506) was patterned on the back of the wafer, and 100nm of chromium was sputtered on top of the photoresist. The photoresist was stripped with acetone to lift the chromium off of the areas of the handle wafer to be etched away. The front of the wafer was covered in photoresist (a layer of HPR 506 and a layer of AZ P4620) for protection, and the exposed portions of the handle wafer were DRIEed through from the back of the wafer.
- 7.) The wafer was diced, and the photoresist on the front was stripped with acetone and the sulfuric acid solution. The buried oxide was etched away from beneath the movable structures in an HF solution, and the die were dried in a critical-point drier.

## 4.2 A Note on Lithography

One of the challenges of masking the etch of the lower teeth with only photoresist was developing a lithography recipe that allowed the photoresist to get deep enough in the trenches between the teeth to protect their sides while it still covered the tops of the teeth properly. AZ P4620 was found to be too viscous to reach a useful depth in trenches 6 $\mu$ m wide. HPR 506 was found to be thin enough to reach the required depth, but when it was spun on the wafer at 500rpm for 10s and 4000rpm for 40s (as it was to pattern the combs and springs in the device layer, and to perform the lift-off of the chromium on the back of the wafer) the tops of the teeth were not properly covered. A solution to this problem was to spin the HPR 506 on the wafer at 500rpm for 10s and 2000rpm for 40s, soft-bake the photoresist by putting the wafer on a hotplate for 90s at 115°C (the same soft-bake performed in the other process steps that involve HPR photoresists), then spin and soft-bake another layer of HPR 506 on top of the first using the same times, speeds, and temperatures. The double-layer of HPR 506 was then exposed to UV light through the mask for approximately twice the amount of time the single layers in the other process steps required, and developed with the same developer – 354.

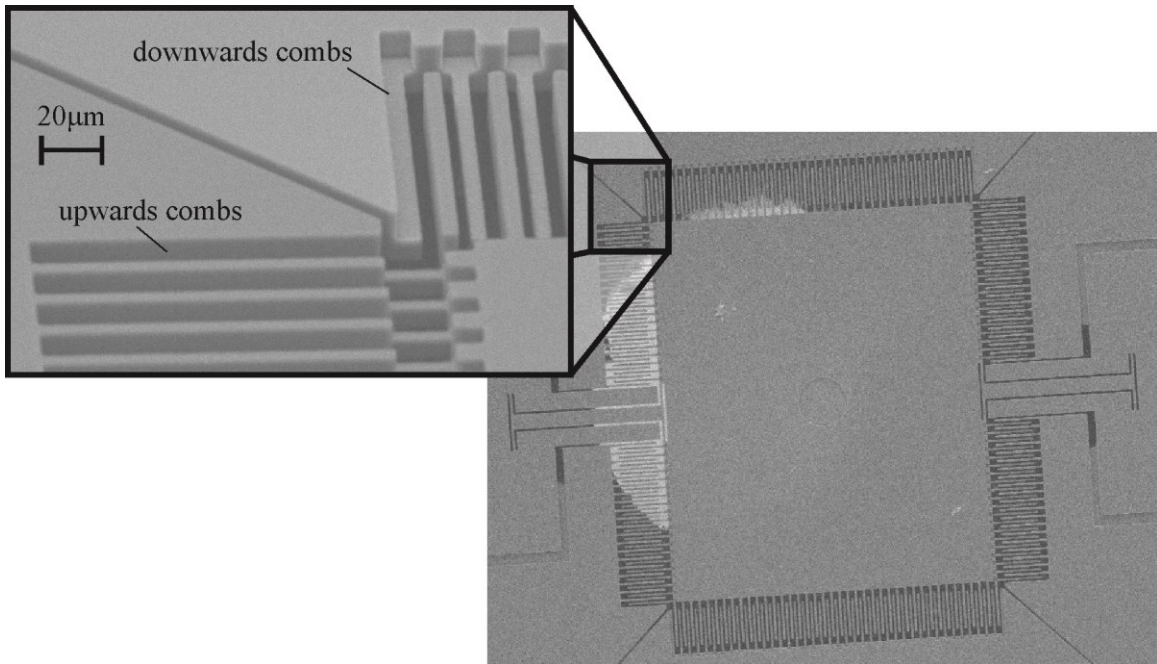


Figure 4.1: A vertical comb drive that has two different sets of opposing comb pairs. One set has its fixed combs positioned above the movable combs; the other set has its fixed combs below the movable combs.

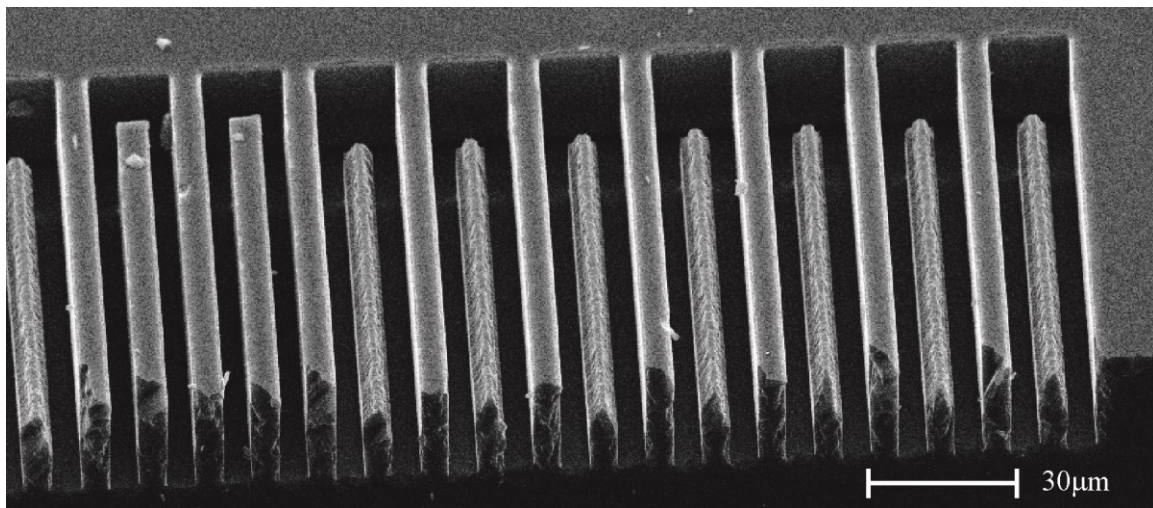


Figure 4.2: A test-etch of the comb teeth into a scrap wafer. Because only the tops of the upper teeth were masked while the tops of the lower teeth were etched down – and the sides of the teeth were not protected – the tops of the lower teeth have been bevelled.

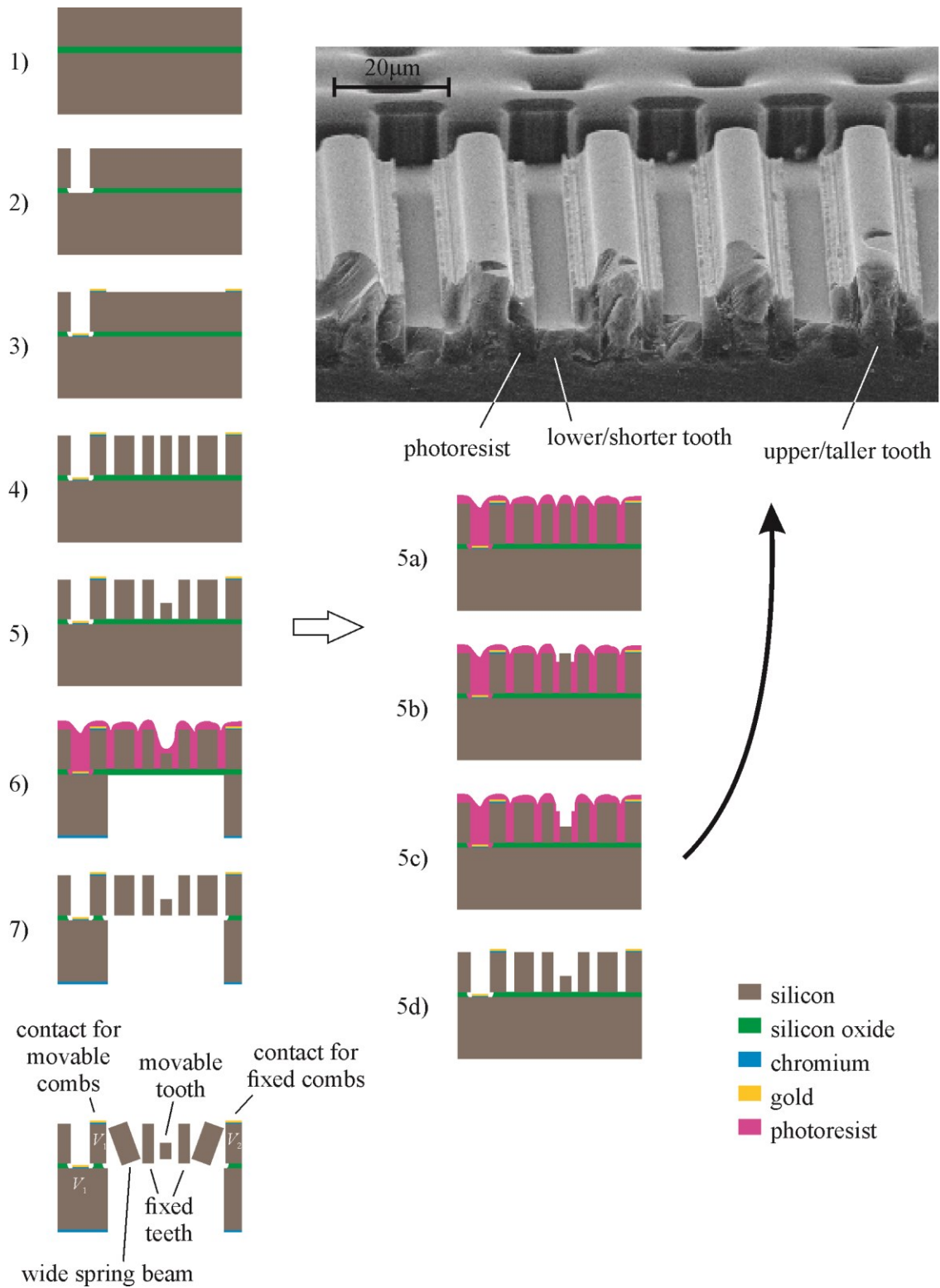


Figure 4.3: A schematic of a simplified cross-section of a die showing the fabrication process steps followed.

# **Chapter 5 : A Preliminary Investigation of the Potential Mechanical Sensitivity of Vertical Comb Drives**

This chapter describes a preliminary step taken in investigating the potential of vertical comb drives to be used as force-compensation mechanisms in interfacial force microscopes, by exploring the lower limit of the stiffness of the springs the comb drives can be fabricated with. The stiffness of their springs will affect the sensitivity of the microscope. The weaker the springs, the smaller the force that is required on the probe for it to reach the displacement detection limit of the feedback control circuit [51]. Six vertical comb drives were fabricated for this study; the dimensions of their spring beams were chosen with the intention of giving them stiffnesses of three different orders of magnitude. The stiffnesses of the fabricated springs were estimated by applying loads to them and measuring their resulting deflections. Weights were applied to the two comb drives with the stiffest springs. Voltages were also applied to them so as to determine the force-voltage relationship for their comb design. Since the other four comb drives had the same comb design, the stiffnesses of their springs could be estimated from the displacements of their movable combs when voltages were applied to them. Finally, the measured spring stiffnesses were compared to stiffnesses predicted with beam equations and finite element simulations.

## **5.1 Prototype Description**

Six vertical comb drives were fabricated for this study. Three of them were fabricated with movable combs that were higher than their opposing fixed combs (so that the movable combs would be pulled downwards when a voltage difference is applied to the comb drive), and three of them were fabricated with movable combs that were lower than the fixed combs (so that the movable combs would be pulled upwards when a voltage difference is applied to the comb drive). All of the comb drives, however, had the same comb design in terms of the number of teeth, the length of the teeth, and the gap between the teeth, so that they would produce the same electrostatic force for a given voltage.

The spring beams of the comb drives were etched at  $45^\circ$  to the  $\langle 100 \rangle$  direction in the silicon to minimize their bulk shear modulus. Three sets of dimensions were chosen for the beams (as shown in figure 5.1) in an attempt to produce springs with stiffnesses of three different orders of magnitude. The “downwards” comb drive with the stiffest springs is shown in figure 2.1. The three sets of dimensions for the springs – as measured in a scanning electron microscope and averaged between the upwards and downwards comb designs – are listed in table 5.1. (The length of the wide spring beams,  $L_b$ , was assumed to retain the designed values, as this dimension, measured between the centre points of the narrow torsion beams, should not be affected by any undercutting in the etch of the silicon.)

## 5.2 Spring Stiffness Predictions

Also listed in table 5.1 are the stiffnesses of the springs that were estimated using (2.2). The bulk shear modulus of the small beams of each spring design was calculated according to their orientation within the silicon and the aspect ratio of their cross-sectional dimensions. They were found to be 53GPa, 52GPa, and 51GPa for the strongest to weakest springs, respectively [53], which corresponded to spring stiffnesses of  $62\mu\text{N}/\mu\text{m}$ ,  $6.8\mu\text{N}/\mu\text{m}$ , and  $0.56\mu\text{N}/\mu\text{m}$ . The spring stiffnesses were also predicted using finite element models made in COMSOL 3.5a. Making use of symmetry, a quarter of each spring arrangement was modelled using stiffness matrix coefficients of  $c_{11} = 166\text{GPa}$ ,  $c_{12} = 64\text{GPa}$ , and  $c_{44} = 80\text{GPa}$ . Loads were then applied to one end of the spring while the other end was fixed, and the resulting displacements were used to calculate the stiffness of the spring using Hooke’s law. The three stiffnesses were calculated to be  $82\mu\text{N}/\mu\text{m}$ ,  $10.2\mu\text{N}/\mu\text{m}$ , and  $0.91\mu\text{N}/\mu\text{m}$ . One reason why the spring stiffnesses predicted with the finite element models are higher than those predicted using (2.2) may be that (2.2) neglects the stiffening effects of the end constraints on the narrow torsion beams of the springs [80].

## 5.3 Spring Stiffness Measurements

The spring constants of the prototypes were measured using the same method – by measuring the displacement of the movable combs while loads were applied to them. A Zygo NewView optical profilometer and a Polytec Topography Measurement System were alternately used to determine the step height between the movable bases of the springs and a fixed reference surface (in an area of the device layer over a remaining portion of the handle wafer, or separated

from the area of the device layer attached to the springs) both before and after the loads were applied.

### ***5.3.1 Characterization of the Stiffest Springs***

The loads were applied to the prototypes with the stiffest springs by placing a series of weights at the centres of their movable combs. Two different methods were used to apply the weights.

#### ***5.3.1.1 Lever Method***

In the first method the weights were applied using a lever mechanism composed of a series of wires attached to a Quater XYZ micropositioner. A schematic of the setup is shown in figure 5.2. A second micropositioner, fitted with an arm that cradled the lever, was used to assist in placing the tip of the lever in the centre of the movable combs. The evenness of the placement could be monitored with the profilometer.

The fulcrum of the lever was moved back and forth along its length to change the weight the tip of the lever applied to the movable combs. Effective masses of 0.010g, 0.020g, 0.030g, and 0.040g were aimed for. The weight the tip applied was measured by placing it on an Acculab Sartorius VIC-303 scale, while the base of the micropositioner was moved through a short range of heights approximately level with the end of the tip. (When the lever mechanism was set up beneath the optical profilometer the base of the micropositioner was approximately level with the base of the silicon chip, as they were adhered to the same platform. The tip of the lever rested on top of the chip, which was around 400 $\mu$ m thick. Because the micropositioner had to be set on a separate stand while the tip of the lever was on the scale, the height of the stand was moved over a range of roughly 2mm, to ensure the angle at which the lever would rest on the movable combs would be covered). 10 measurements were taken of the weight of the tip of the lever while the base of the micropositioner was raised. The uncertainty in the angle at which the lever would rest on the movable combs was found to be small enough that there was no noticeable trend in the variation of the weight the tip applied. It is suspected that the variation came from the lever simply not settling back into the holder on the micropositioner and onto the scale the same way each time it was raised when the base of the micropositioner was moved. The measured weights were multiplied by 9.81m/s<sup>2</sup> to convert them to units of force, and plotted against the resulting displacements of the movable combs measured with the optical profilometer. The plots for the “upwards” comb design and the “downwards” comb design with

the two stiffest springs are shown in figure 5.3. It was presumed that smaller displacements were generally produced with less weight, and, because not all of the ranges of the measured weights fell on the same force-displacement line, it was presumed that the process of placing the tip of the lever in the centre of the movable combs could produce weights outside of the range measured with the scale. Hence the measured spring constants were calculated from linear regression performed between the endpoints of the non-overlapping ranges in order to minimize the distance outside of the ranges the applied weights were estimated to be. The ranges of error for the spring constants were calculated from lines fit to the measured weights above and below the lines calculated for the spring constants. Thus the spring constant of the upwards comb drive was measured to be  $66\mu\text{N}/\mu\text{m}$  ( $58\mu\text{N}/\mu\text{m}$ - $74\mu\text{N}/\mu\text{m}$ ) and the spring constant of the downwards comb drive was measured to be  $70\mu\text{N}/\mu\text{m}$  ( $64\mu\text{N}/\mu\text{m}$ - $85\mu\text{N}/\mu\text{m}$ ).

#### ***5.3.1.2 Direct Method***

In the second method used to calculate the spring constants of the stiffest springs, the scale was mounted onto the stage of the optical profilometer and a micropositioner with a probe was used to push down on the movable combs of the comb drives while the chips containing the comb drives sat on the scale. The measured displacements of the movable combs from their original positions are plotted in figure 5.3 against the weights read from the scale, converted to units of force, while the movable combs were being displaced. The spring constants were determined with linear regression to be  $64\mu\text{N}/\mu\text{m}$  for the upwards comb drive, and  $78\mu\text{N}/\mu\text{m}$  for the downwards comb drive.

#### ***5.3.2 Characterization of the Weaker Springs***

35V was applied between the fixed and movable combs of the two comb drives with the stiffest springs using electrical probes and an Agilent E3647A DC power supply. The movable combs of the upwards comb drive, as measured at the ends of its springs with the optical profilometer, displaced upwards by 97nm. Similarly, the movable combs of the downwards comb drive displaced downwards by 91nm. Using the measured spring constants, the electrostatic force that the comb design provided was estimated and averaged between the two prototypes. Since the electrostatic force is proportional to the square of the applied voltage [81], the electrostatic forces provided by that comb design to the four prototypes with more compliant springs could also be estimated at different voltages. Voltages of 4V, 7V, 9V, and 10V were

applied to the prototypes with the second-weakest springs, and voltages of 1V, 3V, 4V, and 5V were applied to the prototypes with the weakest springs. The corresponding electrostatic forces were calculated and the resulting displacements are plotted against them in figure 5.4. The spring constants of the four prototypes with the more compliant springs were found to be  $6.4\mu\text{N}/\mu\text{m}$  ( $5.7\mu\text{N}/\mu\text{m}$ - $7.5\mu\text{N}/\mu\text{m}$ ) (calculated using the spring constants of the stiff springs measured using the lever mechanism) or  $6.7\mu\text{N}/\mu\text{m}$  (calculated using the spring constants of the stiff springs measured with the scale mounted on the stage of the optical profilometer),  $6.9\mu\text{N}/\mu\text{m}$  ( $6.2\mu\text{N}/\mu\text{m}$ - $8.1\mu\text{N}/\mu\text{m}$ ) or  $7.2\mu\text{N}/\mu\text{m}$ ,  $0.45\mu\text{N}/\mu\text{m}$  ( $0.40\mu\text{N}/\mu\text{m}$ - $0.52\mu\text{N}/\mu\text{m}$ ) or  $0.46\mu\text{N}/\mu\text{m}$ , and  $0.54\mu\text{N}/\mu\text{m}$  ( $0.48\mu\text{N}/\mu\text{m}$ - $0.63\mu\text{N}/\mu\text{m}$ ) or  $0.56\mu\text{N}/\mu\text{m}$ .

#### 5.4 Discussion of Results

The measured values of the spring stiffnesses are generally lower than the predicted values, especially for the weaker spring designs. It is suspected that a critical dimension in (2.2),  $2b_s$  – the width of the torsion beams – may not have been measured accurately. Since the outcome of (2.2) is dependent on the cube of  $2b_s$ , even a small variation in the parameter can have a significant effect on the predicted stiffness. The dimension  $2b_s$  was measured from pictures of the torsion beams taken in a scanning electron microscope. The entire lengths of the beams were included in the pictures so that any variations in their widths could be noted before the places for the measurements of their widths were chosen. Hence for the weaker spring designs the measurement of  $2b_s$  was taken at a lower magnification than those of the stiffer spring designs.

$2b_s$  may also have been over-estimated by a small, constant amount for all of the spring designs, and thus by a larger fraction of the total width for the weaker spring designs. The Bosch DRIE process produces high aspect-ratio trenches by alternating between etch steps and deposition steps [79]. In the deposition steps the wafer is coated in a polymer to protect the sides of the trenches from further etching. The etching plasma is then directed towards the bottoms of the trenches, and once it has broken through the polymer layer it etches the silicon isotropically. These short isotropic etches produce scallops in the sidewalls of the trenches, as shown in figure 5.5. Hence the torsion beams are likely a little narrower than what was measured from a top view of them in the scanning electron microscope. The sidewall scallops were estimated to have undercut all of the dimensions of the springs by  $0.2\mu\text{m}$ . Factoring this into (2.2) and applying it to the finite element model of the weakest spring design produces predicted stiffness values of

0.47 $\mu\text{N}/\mu\text{m}$  and 0.78 $\mu\text{N}/\mu\text{m}$ , respectively – which are significantly closer to the measured stiffness values.

Nonetheless, it seems that vertical comb drives with spring stiffnesses of three different orders of magnitude were able to be fabricated using the dimensions chosen for the “I”-shaped spring design, and the lowest spring stiffnesses achieved were measured to be 0.45 $\mu\text{N}/\mu\text{m}$  (0.40 $\mu\text{N}/\mu\text{m}$ -0.52 $\mu\text{N}/\mu\text{m}$ ) or 0.46 $\mu\text{N}/\mu\text{m}$  and 0.54 $\mu\text{N}/\mu\text{m}$  (0.48 $\mu\text{N}/\mu\text{m}$ -0.63 $\mu\text{N}/\mu\text{m}$ ) or 0.56 $\mu\text{N}/\mu\text{m}$ . If, for instance, an interferometer that could detect displacements as small as 1 $\text{\AA}$  were used to monitor the position of the movable combs of these comb drives, forces applied to the movable combs as small as 0.040nN-0.063nN could be detected – which is a good first step towards designing comb drives that are to aid in measuring interfacial forces.

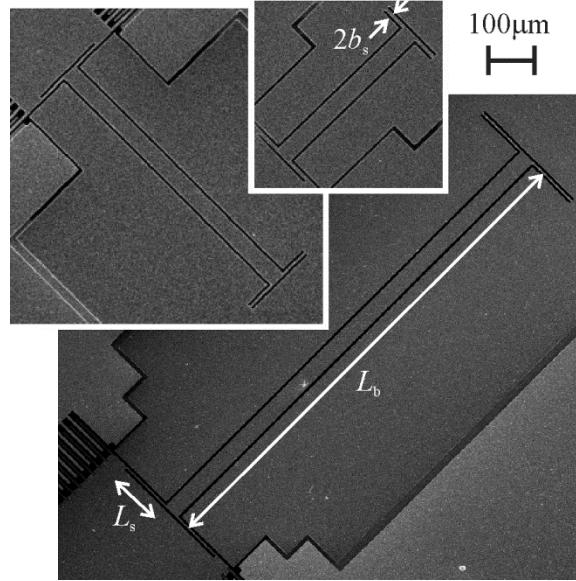


Figure 5.1: The three spring designs studied. The comb drives were designed to have one of these on each side of the movable combs. The thickness of the narrow spring beams,  $2a_s$ , was equal to the thickness of the device layer.

Table 5.1: The predicted and measured stiffnesses of the three spring designs.

Spring Design	Spring Dimensions ( $\mu\text{m}$ )				Predicted Stiffness ( $\mu\text{N}/\mu\text{m}$ )		Measured Stiffness ( $\mu\text{N}/\mu\text{m}$ )	
	$2a_s$	$2b_s$	$L_s$	$L_b$	Equation (2.2)	Finite Element	“Up” Drive	“Down” Drive
1	20.5	6.251	57.58	400	62	82	66 (58-74) or 64	70 (64-85) or 78
2	20.5	4.629	72.26	700	6.8	10.2	6.4 (5.7-7.5) or 6.7	6.9 (6.2-8.1) or 7.2
3	20.5	3.497	131.4	1200	0.56	0.91	0.45 (0.40-0.52) or 0.46	0.54 (0.48-0.63) or 0.56

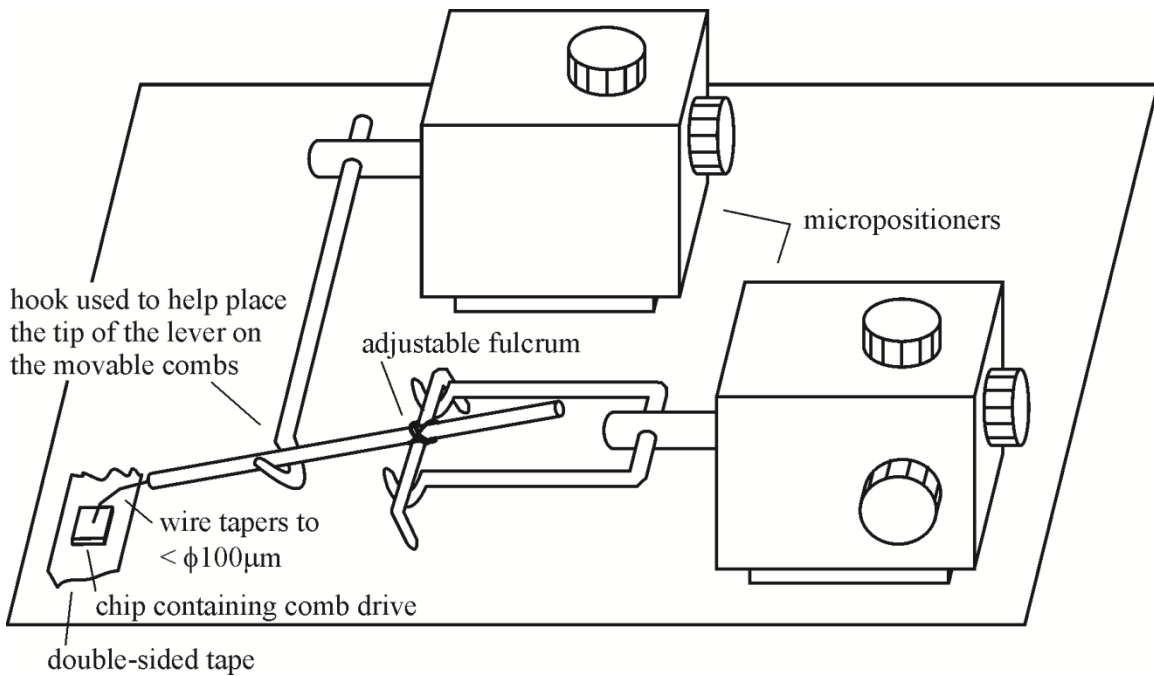


Figure 5.2: The mechanism used to apply different weights to the movable combs of the comb drives with the stiffest springs.

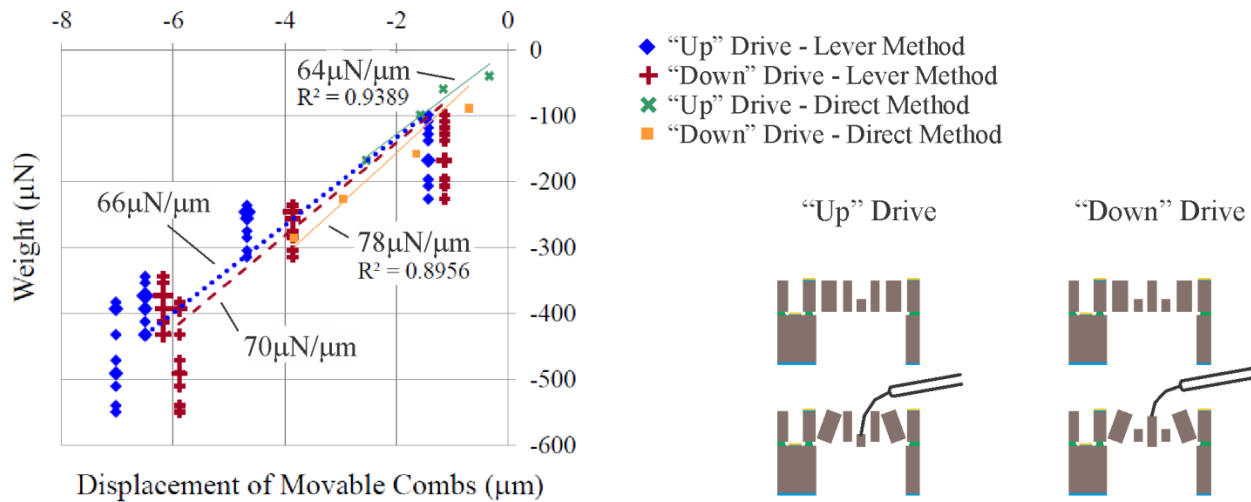
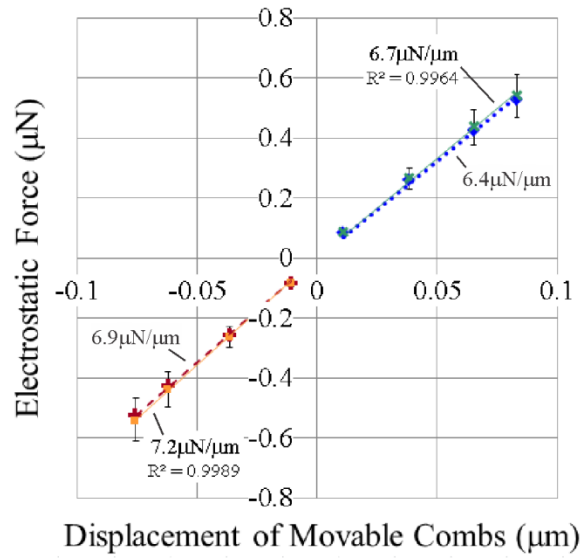
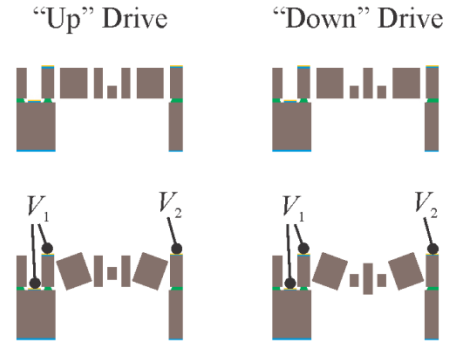


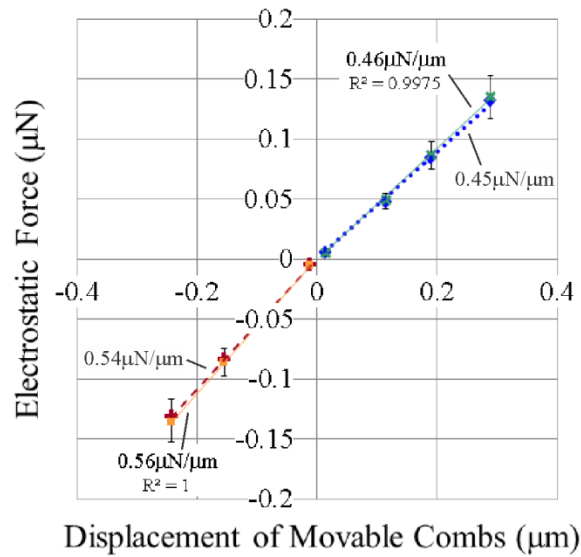
Figure 5.3: The comparison of the displacements of the movable combs to the weights that were applied to them, from which the spring constants of the stiffest springs were calculated. A few of the data points have been made larger to indicate that those values of the weights were recorded two or three times.



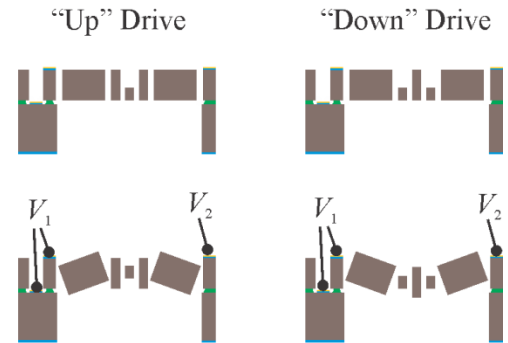
- ◆ “Up” Drive - Lever Method
- ✚ “Down” Drive - Lever Method
- ✕ “Up” Drive - Direct Method
- “Down” Drive - Direct Method



(a)



- ◆ “Up” Drive - Lever Method
- ✚ “Down” Drive - Lever Method
- ✕ “Up” Drive - Direct Method
- “Down” Drive - Direct Method



(b)

Figure 5.4: Comparisons of the displacements of the movable combs to the electrostatic forces that were applied to them, from which the spring constants of the (a) second-weakest, and (b) weakest springs were calculated.

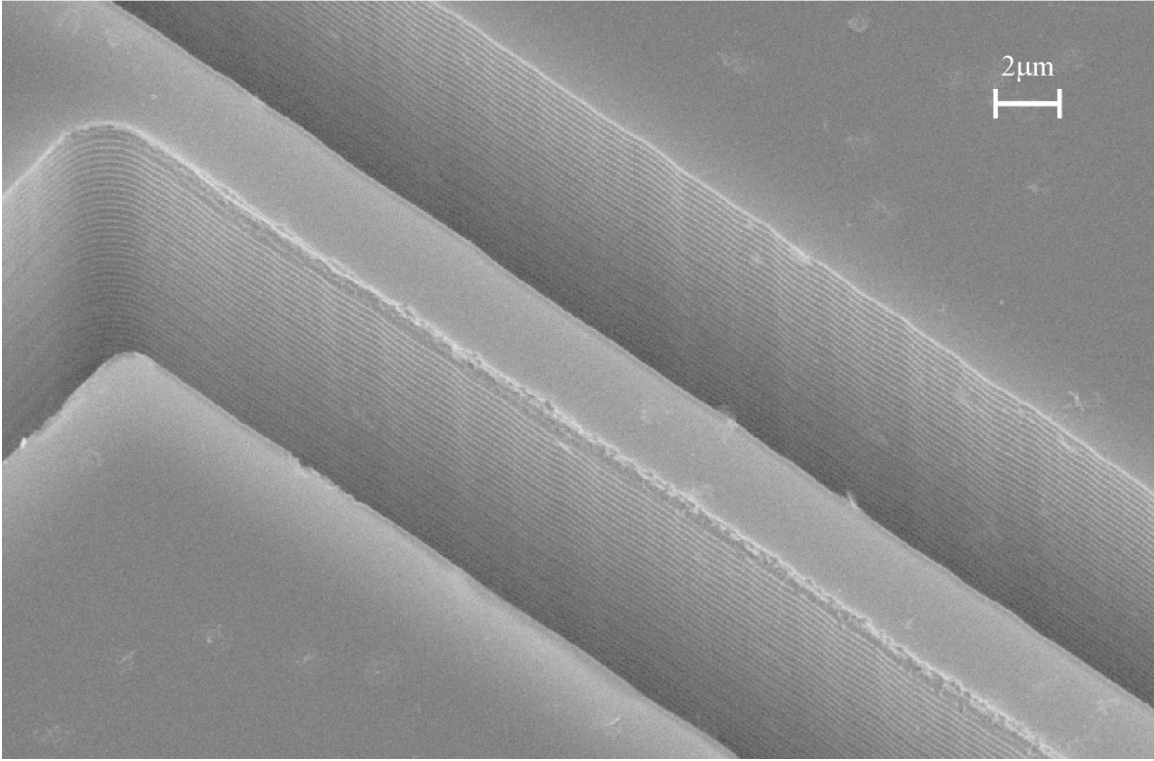


Figure 5.5: The scalloped sidewalls left by the Bosch process on the narrowest spring beams.

# Chapter 6 : A Study of the Effect of the Fringe Fields on the Electrostatic Force in Vertical Comb Drives

The equation that describes the relationship between the applied voltage and the resulting electrostatic force within comb drives is often used to assist in choosing the dimensions for their design. This chapter re-examines how some of these dimensions – particularly the cross-sectional dimensions of the comb teeth – affect this relationship in vertical comb drives. The electrostatic forces in several vertical comb drives fabricated for this study were measured and compared to predictions made with four different mathematical models in order to explore the amount of complexity required within a model to accurately predict the electrostatic forces in the comb drives. The basic case where the opposing teeth maintain the same relative height along their length, in the absence of a ground plane, was considered.

## 6.1 Derivation of Basic Electrostatic Force Equation

The fixed and movable combs of a comb drive, being isolated conductors, form a capacitor when they are charged by the voltage difference applied between them. The fixed and movable combs have equal and opposite charges of  $+q_e$  and  $-q_e$ , although the total charge between them is considered to be  $q_e$ . The capacitance,  $C$ , of a capacitor is the proportionality constant that relates the charge on its opposing plates to the voltage difference,  $V$  (as in (6.1)), and it is dependant only on the physical geometry of the plates [82]:

$$q_e = C V . \tag{6.1}$$

The physical geometry of the opposing combs in a comb drive is usually considered to consist of a number of overlapping parallel plates, that are assumed to be large enough and close enough together that the electric fields between them are uniform and confined to their overlapping regions (that is, the bending of the electric fields around the corners of the comb teeth can be ignored) [82]. The expression most often used to describe the capacitance between parallel plates is that of (6.2), where  $\epsilon$  is the permittivity of the medium between the plates,  $g$  is the lateral gap between the plates (shown in figure 6.1), and  $A_c$  is their overlapping area:

$$C = \frac{\epsilon A_c}{g}. \quad (6.2)$$

Summing the amount of work done to charge the combs against an increasing voltage difference, and using the relationship between the charge and voltage difference given in (6.1), the energy stored in a capacitor,  $U$ , no matter its geometry, can be described as [82]:

$$U = \frac{1}{2} C V^2. \quad (6.3)$$

The net electrostatic force exerted on the movable combs of a comb drive,  $F_e$ , is typically found by considering the change in the electric potential energy between the comb teeth as they slide past each other. Taking the derivative of the energy with respect to the displacement of the movable combs,  $z$ , gives (6.4) for the portion of  $z$  where the teeth are partially overlapping, and zero everywhere else. The electrostatic force acts on the movable combs to pull them towards positions of increased capacitance. The two other parameters that represent the overlapping area of the opposing combs are the total number of movable teeth,  $n$  (assuming there are enough fixed teeth that they exert electrostatic forces on both sides of each movable tooth), and the overlapping length of the teeth,  $L_t$ :

$$F_e = \frac{\partial U}{\partial z} = \frac{1}{2} \frac{\partial C}{\partial z} V^2 = \frac{\epsilon n L_t}{g} V^2. \quad (6.4)$$

(6.4) is the first estimate of the relationship between the electrostatic force,  $F_e$ , and the voltage applied between the fixed and movable combs of a comb drive,  $V$ . It is often used to assist in deciding what the gap between the teeth should be, how long the teeth should be, and how many teeth there should be in a particular comb drive design.

## 6.2 First Estimate of the Effect of the Fringe Fields on the Electrostatic Force

Fabrication techniques for micromachines such as comb drives tend to be limited to producing structures that are relatively thin in the direction perpendicular to the surface of the substrate they are machined on. Hence comb teeth are usually made to be thin, and long in a

direction parallel to their substrate. If their fixed and movable combs are offset from each other parallel to the substrate surface (as in a lateral comb drive), there is a relatively long range over which the movable combs can displace before their ends approach the ends of the fixed teeth and restrict the overlapping region where the electric field between them can be considered to be uniform, and the electrostatic force can be described by (6.4) [25, 83, 84]. On the other hand, if the fixed and movable combs are offset from each other perpendicular to the substrate (as in a vertical comb drive), there is a relatively short range over which the necessary amount of overlap can be maintained.

The failure of (6.4) to include the fringe fields around the comb teeth comes from the failure of (6.2) to include the fringe fields around the comb teeth. A method involving Schwartz-Christoffel transformations [85] has been heralded as providing an exact calculation of the capacitance between two-dimensional representations of aligned parallel plates [86, 87]. It finds relations that transform the co-ordinates of the plates, being boundaries of the electric field (and between which the electric field lines are unknown curves), into co-ordinates in a new plane where the entire electric field is contained directly between the plates (between which the field lines are uniformly-spaced straight lines). The capacitance between the idealized plates can then be calculated with (6.2), using the determined transformation relations to find the dimensions of the idealized plates from the dimensions of the real plates.

Unfortunately, the Schwartz-Christoffel transformation method for calculating capacitance cannot be expressed as a single equation, so its derivative cannot simply be taken and used to calculate the electrostatic force between the plates as in (6.4). Much of the calculation process must be done numerically, and even further numerical steps are needed if the widths of the plates are to be included or plates of differing thicknesses are being considered [86]. The method is also limited to the analysis of parallel plates that have their centres aligned with each other. The centres of opposing comb teeth need to be offset from each other if there is to be a net force between them.

One attempt that has been made [88, 89] at including the fringe electric fields in the calculation of the electrostatic force in vertical comb drives involves the conformal mapping of a two-dimensional model of half of a unit comb drive. The model is comprised of the space between zero-width cross-sections of the opposing halves of one fixed comb tooth and one movable comb tooth, as in those models shown in figure 6.2. The end result of this work is

effectively a function,  $f$ , that is appended to (6.4), that describes the effect of the fringe field on the electrostatic force. It predicts a changing electrostatic force over  $z$ , and is able to predict a force in the ranges of  $z$  where the comb teeth do not partially overlap. The form of  $f$  that was derived,  $f_1$ , is shown in (6.5) and is based on the positions of the tops and bottoms of the comb teeth ( $a'$ ,  $b'$ ,  $c'$ , and  $d'$  – relative to a scale downwards from  $d'$ ), or, the relative position of the teeth, the thicknesses of the teeth, and the gap between them ( $z$ ,  $t_s$ ,  $t_T$ , and  $g$ ):

$$F_e = \frac{\varepsilon n L_t V^2}{g} f_1(g, t_s, t_T, z) \quad (6.5)$$

$$= \frac{\varepsilon n L_t V^2}{g} \cdot \frac{\pi^2 \left( a \frac{b-d}{a-d} - b \frac{a-c}{b-c} \right)}{4(a-b) \left\{ F[\delta(u=0), q] + F[\kappa(u=0), q] \right\}^2}$$

where

$$q = \sqrt{\frac{(b-c)(a-d)}{(a-c)(b-d)}} \quad (6.5a)$$

$$\delta = \sin^{-1} \sqrt{\frac{(b-d)(u-c)}{(b-c)(u-d)}} \quad (6.5b)$$

$$\kappa = \sin^{-1} \sqrt{\frac{(a-c)(b-u)}{(b-c)(a-u)}} \quad (6.5c)$$

and  $F$  is the incomplete elliptic function of the first kind – one representation of which is given in (6.5d) [90]. It must be approximated numerically:

$$F(\varphi, k) = \int_0^{\sin \varphi} \frac{dp}{\sqrt{(1-p^2)(1-k^2 p^2)}}. \quad (6.5d)$$

The remaining variables –  $a$ ,  $b$ ,  $c$ , and  $d$  – can be related to the physical endpoints of the teeth through (6.5e-h):

$$a = e^{\pi a'/g} = e^{\pi(b'+t_s)/g} \quad (6.5e)$$

$$b = e^{\pi b'/g} \quad (6.5f)$$

$$c = -e^{\pi c'/g} = -e^{-\pi t_T/g} \quad (6.5g)$$

$$d = -e^{\pi d'/g} = -1. \quad (6.5h)$$

Finally, relating  $\mathbf{b}'$  to  $\mathbf{z}$  is trivial – the co-ordinate system chosen for the work presented here has its origin at the midpoint of the taller comb teeth, and increases as the midpoint of the shorter comb teeth travels (relative to the taller teeth) in the direction outwardly normal to the substrate surface, thus:

$$\mathbf{b}' = -\mathbf{z} - \left( \frac{t_T + t_s}{2} \right). \quad (6.5i)$$

(6.5) is shown graphically in figure 6.3 for the cases where  $g/t_T = 1/10$  and  $1/2$ , and where the fixed and movable tooth are the same thickness, and where one is a quarter of the thickness of the other. (These are values that the dimensions of typical microfabricated vertical comb teeth are expected to fall between.) The relative position of the teeth is varied from where the vertical midpoints of the teeth are aligned horizontally, to a little beyond where the teeth no longer overlap (for the  $t_s/t_T = 1$  case they no longer overlap at  $z/t_T = -1$ , and for the  $t_s/t_T = 1/4$  case they no longer overlap at  $z/t_T = -0.625$ ). Since the attractive force on a tooth pulls it towards the vertical midpoints of its opposing teeth, the force on the tooth always acts in the opposite direction to its position vector (that is, if the positions of the teeth were varied around  $z/t_T \geq 0$ , the forces on the shorter tooth would be of the same magnitude but in the negative direction). In the figure, (6.5) has been non-dimensionalized with respect to (6.4) (which produces a straight line at a force of 1 while the teeth partially overlap). Not surprisingly, the figure shows that a larger gap between the teeth lowers the force between them, and also lowers the rate of change of the force as the teeth come to completely overlap, and as they move to not overlap at all. Having one tooth shorter than the other decreases the maximum force and narrows the distance over which the force acts, as there is a longer range of travel where the teeth completely overlap.

## 6.3 Addition of Tooth Width to Electrostatic Force Calculations

### 6.3.1 Verification of Finite Element Models

The derivation of (6.5) assumes that the comb teeth are narrow enough that their width does not affect the electrostatic forces between them. Having wider teeth is advantageous during fabrication process development, however, as they are more likely to survive being etched if the amount of undercut of the masking layer to expect is unknown, and they are less likely to break during their release from the substrate. Hence finite element models of the air around the cross-section of a pair of comb teeth were developed in the program COMSOL 3.5a to calculate the capacitances of different tooth configurations. Initially, the models were made with zero-width teeth so as to compare their results with those in the literature.

A finite element model with a unit potential difference applied between an example pair of teeth (that were separated by a gap equal to half their thickness) calculated the same capacitance of  $2.89 \times 10^{-13} \text{F/cm}$  as the Schwartz-Christoffel method [85]. In subsequent models, to represent pairs of teeth that are a part of an array of teeth, only the space around half of each tooth was included, and symmetric conditions were applied to the boundaries extending from the teeth along their vertical axes. These models were used to calculate a number of capacitances for different relative vertical positions of the teeth. The differences between the capacitances were taken, divided by the respective changes in position, and multiplied by “ $\frac{1}{2}V^2$ ,” as in (6.4). The resulting electrostatic forces have been plotted against those predicted by (6.5) in figure 6.3. On average, they deviate from those predicted by (6.5) by 0.6% of the maximum force predicted by (6.4), with a maximum of 2.8%.

### 6.3.2 Addition of Width to Plate Model

The width of the comb teeth was added to the finite element models by extending the discretized space horizontally to half the width of both teeth, as shown in figure 6.4. The precise dimensions chosen for the models were those measured from a vertical comb drive that was fabricated for this study, which is shown in figure 6.5. The comb drive has 160 movable teeth, and the four beams that extend in opposing directions from the movable combs act as its springs. The overlapping length of the teeth was estimated from pictures taken in a scanning electron microscope to be  $99.24 \mu\text{m}$ , and the relative width of, gap between, and thickness of the teeth are those shown in figure 6.6 of  $0.260t_T$ ,  $0.276t_T$ , and  $0.384t_T$ , respectively, although the thickness of

the shorter teeth was determined by subtracting the depth of the etch of their tops, measured with a Zygo NewView optical profilometer, from the thickness of the taller teeth.

Figure 6.7 shows the electrostatic forces predicted for this comb drive using (6.5) and using the capacitances obtained from the finite element models. The largest difference between the two predictions occurs when the comb teeth no longer overlap in the vertical direction. When the top of one tooth is facing the bottom of the other, including the width of the teeth in the calculation increases the area over which the electric charge can accumulate, resulting in a higher predicted electrostatic force.

#### **6.4 Electrostatic Force Measurements**

20V was applied to the fixed combs of the comb drive using electrical probes and an Agilent E3647A DC power supply. The movable combs and the handle wafer were grounded. The optical profilometer was used to measure the relative heights of the opposing combs while the voltage was applied, as well as the step height between the movable bases of the springs and a fixed reference surface (in an area of the device layer over a remaining portion of the handle wafer) before and after the voltage was applied. 20V was found to raise the ends of the springs by an average of 44nm.

This displacement was used to calculate the electrostatic force generated by the 20V by multiplying it by the measured stiffness of the springs, as the electrostatic force would be equal to the restoring force provided by the springs after the voltage had drawn the movable combs up to their new position. The stiffness of the springs was determined the same way as in Chapter 5 – by using an optical profilometer to measure the displacement of the movable combs while a series of four weights were applied to their centre. Two different methods were used to apply the weights. In the first method, weights were applied using a lever mechanism; the amount of weight the tip of the lever applied was measured by placing it on a scale. 10 measurements of each weight were taken and multiplied by  $9.81\text{m/s}^2$  to convert them to units of force, and plotted against the resulting displacement of the movable combs in figure 6.8. It was presumed that smaller displacements were produced with less weight, so the spring constant was calculated from linear regression performed between the values of the measured weights in the parts of the ranges of the measured weights that overlapped. The ranges of error for the spring constant was calculated from lines fit to the measured weights above and below the lines calculated for the spring constants. In the second method used to measure the stiffness of the spring, the scale was

mounted onto the stage of the optical profilometer and a micropositioner with a probe was used to push down on the movable combs of the comb drive while the chip containing the comb drive sat on the scale. The measured displacements of the movable combs are plotted in figure 6.8 against the weights read from the scale. The spring constant was determined from linear regression between the points.

The spring constant of the comb drive that underwent 44nm of displacement at 20V was thus measured to be 109 $\mu$ N/ $\mu$ m (96 $\mu$ N/ $\mu$ m-122 $\mu$ N/ $\mu$ m) or 118 $\mu$ N/ $\mu$ m. These are reasonably close to the 113 $\mu$ N/ $\mu$ m calculated using (6.6):

$$k_{z+} = \frac{4 E w_b t_b^3}{L^3} \quad (6.6)$$

where  $E$  is the modulus of elasticity of the silicon,  $L$  is the length of the spring beams,  $w_b$  is the width of the spring beams, and  $t_b$  is their thickness. The spring beams were oriented along the  $\langle 100 \rangle$  directions of the (100) device layer of the wafer in order to minimize their modulus of elasticity, which was taken to be 130.2GPa [53]. The length, width, and thickness of the beams were measured in a scanning electron microscope to be 1065 $\mu$ m, 30.34 $\mu$ m, and 20.5 $\mu$ m, respectively. The measured spring constants are also reasonably close to the 107 $\mu$ N/ $\mu$ m calculated from the displacement of a finite element model of the movable combs when different weights were applied to its centre. Using the measured spring constants, the voltage difference was estimated to have generated 4.8 $\mu$ N (4.3 $\mu$ N-5.4 $\mu$ N) or 5.2 $\mu$ N of electrostatic force between the opposing combs. This measured electrostatic force has been non-dimensionalized with respect to (6.4) and plotted in figure 6.7 against (6.5) and the forces predicted with the non-zero width plate model. The measured force seems to coincide with the predicted forces rather well, although there is not a large difference between the two predictions at this relative height of the teeth.

To increase the range of relative heights of the opposing comb teeth over which the electrostatic force could be measured, another set of vertical comb drives were designed that had their “fixed” combs also attached to springs, so that the probes used to apply the voltages to the fixed combs could also be used to push them downwards to create different vertical offsets between them and the movable combs. No adjustments to the fabrication process for the comb

drives were needed, only the outlines of the comb drives that were etched through the device layer of the SOI wafer were changed. As can be seen in figure 6.9, the springs were re-designed so that the two “un-fixed” combs could fit on either side of the movable combs. The vertical compliance of these springs comes from the twisting of the smaller spring beams [52], which allows the larger beam that connects them to be wider – which helps resist the tilting of the movable combs about the axis of the wide beams.

The displacements of the movable combs in the new comb drives were measured in the same way as the displacement of the movable combs in the first comb drive; however, the vertical offset between the teeth of the new comb drives was set by the height at which the Quater XYZ micropositioners held the probes that applied the voltage to the un-fixed combs. Before voltages were applied to the combs, the optical profilometer was used to ensure that the two un-fixed combs were pushed down evenly. The difference in their height was kept below 500nm, or approximately  $0.024t_T$ . Their relative position to the movable combs when the voltage was applied was then taken as an average between them.

The comb drive shown in figure 6.9 has 80 movable teeth. The overlapping length of the teeth was measured to be  $98.26\mu\text{m}$ , and the relative width of, gap between, and thickness of the teeth are  $0.241t_T$ ,  $0.296t_T$ , and  $0.365t_T$ , respectively. The stiffness of its springs was measured with the scale on the stage of the optical profilometer to be  $75\mu\text{N}/\mu\text{m}$ , and with the lever mechanism to be  $63\mu\text{N}/\mu\text{m}$  ( $54\mu\text{N}/\mu\text{m}$ - $79\mu\text{N}/\mu\text{m}$ ). In this case, because not all of the ranges of the measured weights fell on the same force-displacement line, it was presumed that the process of placing the tip of the lever in the centre of the movable combs could produce weights outside of the range measured previously with the scale, so the measured spring constants were calculated from linear regression performed between the endpoints of the non-overlapping ranges in order to minimize the distance outside of the ranges the applied weights were estimated to be. The range of error for the spring constant was still calculated from lines fit to the measured weights above and below the line calculated for the spring constant. The measured spring stiffnesses are close to the  $71\mu\text{N}/\mu\text{m}$  calculated from a finite element model of this spring design, although a little less so to the  $53\mu\text{N}/\mu\text{m}$  calculated using (2.2). ( $2a_s$ ,  $2b_s$ , and  $L_s$  were measured in a scanning electron microscope to be  $20.5\mu\text{m}$ ,  $5.931\mu\text{m}$ , and  $58.74\mu\text{m}$ , respectively, while  $L_b$  was assumed to retain the designed value of  $400\mu\text{m}$ . The bulk shear modulus of the torsion beams was calculated according to the aspect ratio of their cross-sectional dimensions

and their orientation within the silicon [53]. They were oriented at  $45^\circ$  to the  $\langle 100 \rangle$  direction in the device layer of the wafer so as to minimize the bulk shear modulus, which was calculated to be 53GPa.)

35V was applied between the opposing combs of the comb drive at each position its un-fixed combs were held at. The resulting forces that were measured using the optical profilometer are shown in figure 6.10. In this comb drive design the movable teeth are the shorter teeth, so they were pulled up towards the centres of the un-fixed teeth when the un-fixed teeth were held only slightly below their fabricated positions, and the movable teeth were pulled downwards when the un-fixed teeth were pushed down so that their centres were below those of the movable teeth.

The method of varying the relative heights of the combs by pushing down “un-fixed” combs also allowed forces to be measured in a comb drive that has opposing comb teeth of the same thickness. This final comb drive prototype also has 80 movable teeth, which overlap the un-fixed teeth by  $99.98\mu\text{m}$ , while the relative width of the teeth is  $0.234t_T$ , and the gap between them is  $0.300t_T$ . The stiffness of its springs was measured with the lever mechanism to be  $68\mu\text{N}/\mu\text{m}$  ( $60\mu\text{N}/\mu\text{m}$ - $87\mu\text{N}/\mu\text{m}$ ) and with the scale on the stage of the optical profilometer to be  $70\mu\text{N}/\mu\text{m}$ , which correspond well to the  $69\mu\text{N}/\mu\text{m}$  calculated from a finite element model of its springs, although it corresponds a little less so to the  $50\mu\text{N}/\mu\text{m}$  calculated from (2.2), where  $2a_s$ ,  $2b_s$ , and  $L_s$  were measured to be  $20.5\mu\text{m}$ ,  $5.789\mu\text{m}$ , and  $57.02\mu\text{m}$ , respectively, while  $L_b$  was again assumed to be  $400\mu\text{m}$ , and  $G$  was calculated to be 52GPa. 35V was applied between the opposing combs of the comb drive at each position its un-fixed combs were held at. The resulting forces that were measured using the optical profilometer are shown in figure 6.11. Since in this comb drive design all of the teeth are the same thickness, the force on the movable teeth was plotted, and again, this force acted in the negative direction as the movable teeth remained above the un-fixed teeth as the un-fixed teeth were pushed down by the probes.

## 6.5 Addition of End of Row to Model

The magnitudes of the measured electrostatic forces seem to lie between those predicted with the finite element models of the unit comb drives and the zero-width approximation of (6.5). This is particularly noticeable for the comb drive that had fixed and movable teeth of the same thickness, as the two different predictions are very close to each other for the other two

comb drives that had movable teeth that were around four tenths of the thickness of their fixed teeth.

The 2-D finite element models of the cross-sections of the comb teeth were expanded as shown in figure 6.12 to include half of a row of teeth (that is, 20 movable teeth and their counterparts) and the cross-section of the area of the device layer at the end of the row of teeth – to a length of half of the dimension  $s$ , shown in figure 6.9. Symmetric boundary conditions were applied to the two ends of the models, and capacitances were calculated at different relative heights of the teeth as before. The resulting electrostatic forces were non-dimensionalized with respect to (6.4), and plotted in figures 6.10 and 6.11. This final prediction of the electrostatic forces seems to match well with those measured from the fabricated comb drives. As can be seen from the equipotential lines in figure 6.12, the portion of the device layer at the end of the row of teeth appears to be drawing the electric field away from the tops and bottoms of the teeth. Hence for the ranges of relative heights of the teeth where the width of the teeth is expected to affect the electrostatic force between them, including a portion of the electrodes around the teeth in the model seems necessary to determine how much the width of the teeth will affect the electrostatic force.

## **6.6 Discussion of the Significance of Including the Fringe Fields in the Electrostatic Force Calculation**

Besides allowing an estimate to be made of the complexity of the mathematical model required to accurately predict the electrostatic forces within vertical comb drives, the collection of measured electrostatic forces was valuable in another way: it indicated that the comb drives fabricated using the process detailed in Chapter 4 will only generate about half the electrostatic force for any given voltage than that predicted by (6.4) – the equation traditionally used to determine the dimensions of the comb teeth required for a particular force-voltage relationship. For example, if the comb drive shown in figure 6.5 were used as a force-compensation mechanism, and it were possible to detect a change in the compensation voltage as small as 10mV, theoretically, once an external force had pushed the movable combs to the displacement detection limit of the system, the comb drive could compensate for changes in the force on the movable combs as small as 1pN (or 5nN, if, for instance, 19V had already been applied to pull against 4 $\mu$ N). These values were obtained by adding a factor of 0.5 to (6.4). If the effect of the

fringe fields were to be neglected, such a comb drive would be designed to have, for example, half the number of comb teeth that it needed to achieve these forces.

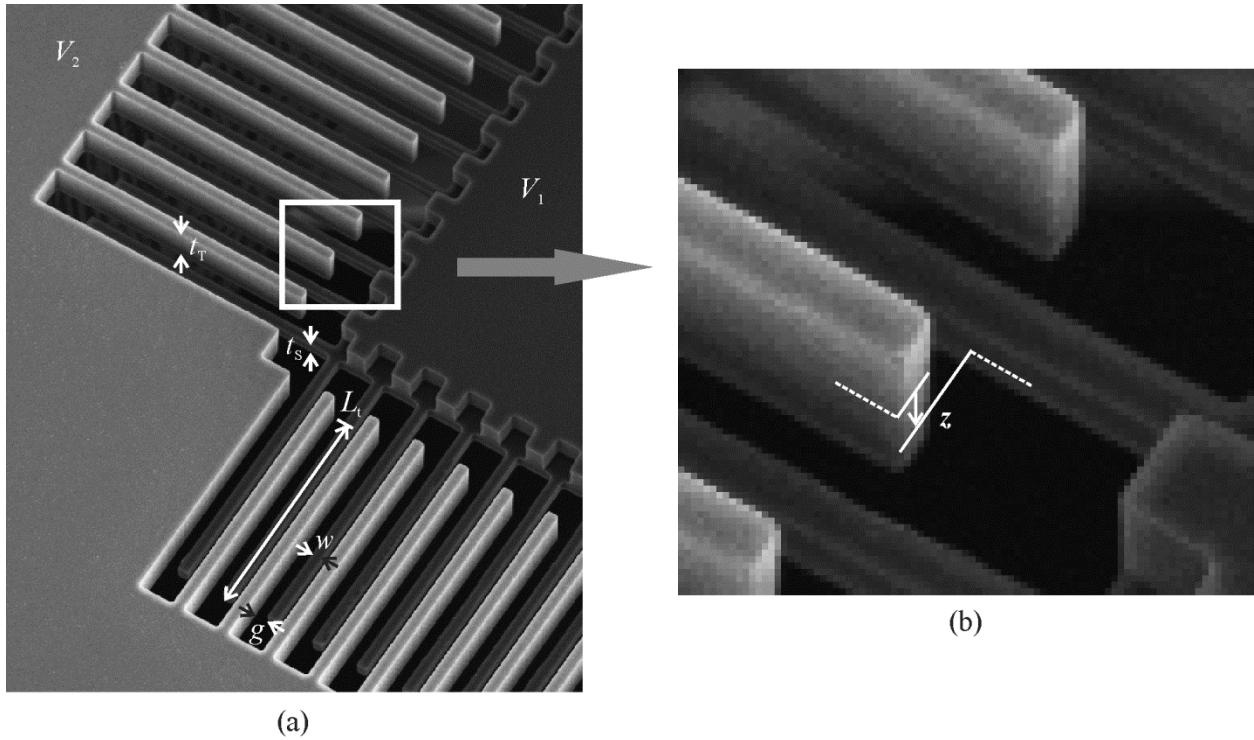


Figure 6.1: Some of the dimensions of the comb teeth that are expected to affect the electrostatic forces generated between them. (b) is an enlarged view of the area indicated in (a). It should be noted that “ $t_S$ ” refers to the thickness of the shorter teeth and “ $t_T$ ” to the thickness of the taller teeth, regardless of which are the fixed teeth and which are the movable teeth.

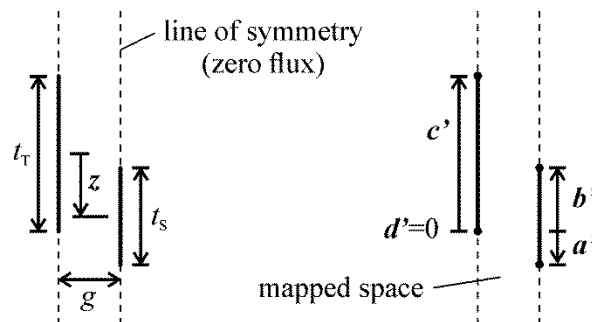


Figure 6.2: Two different representations of the two-dimensional model of the space between opposing teeth of negligible width.

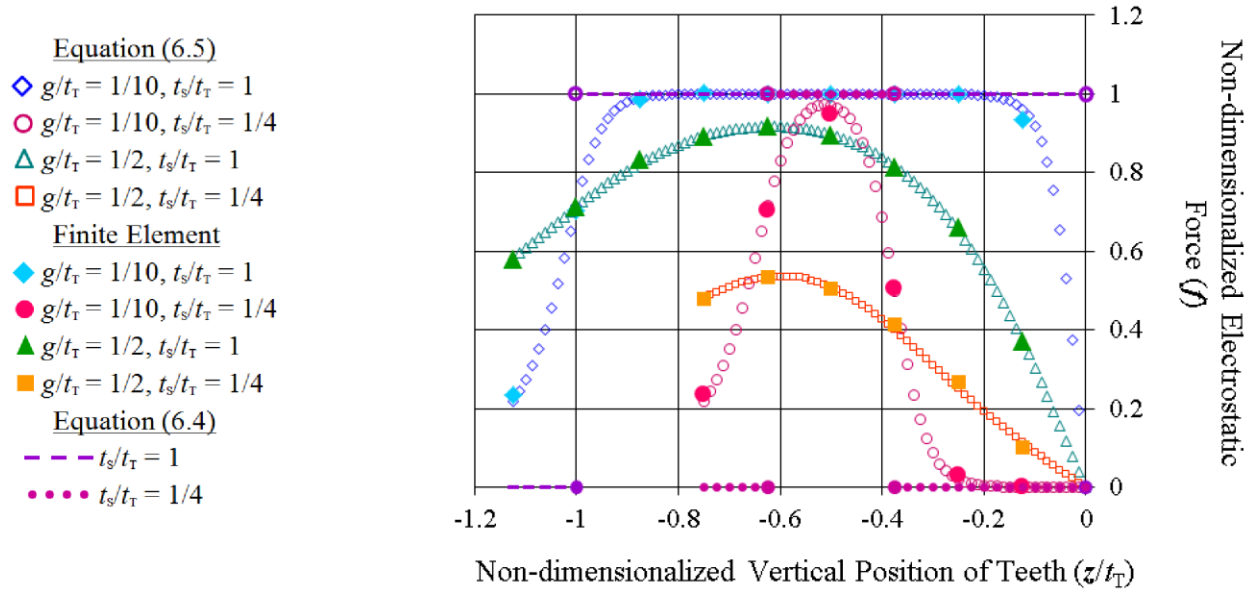


Figure 6.3: Different predictions of the fraction of the maximum electrostatic force that acts on the movable combs over their displacement.

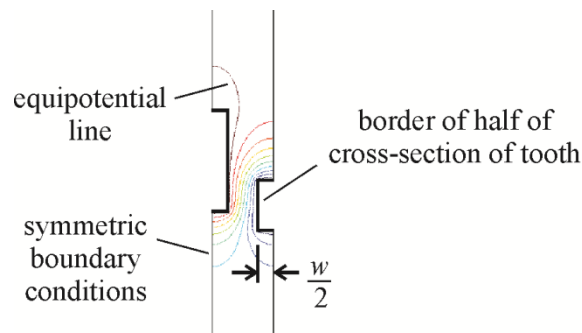


Figure 6.4: One of the finite element models that includes the width of the comb teeth.

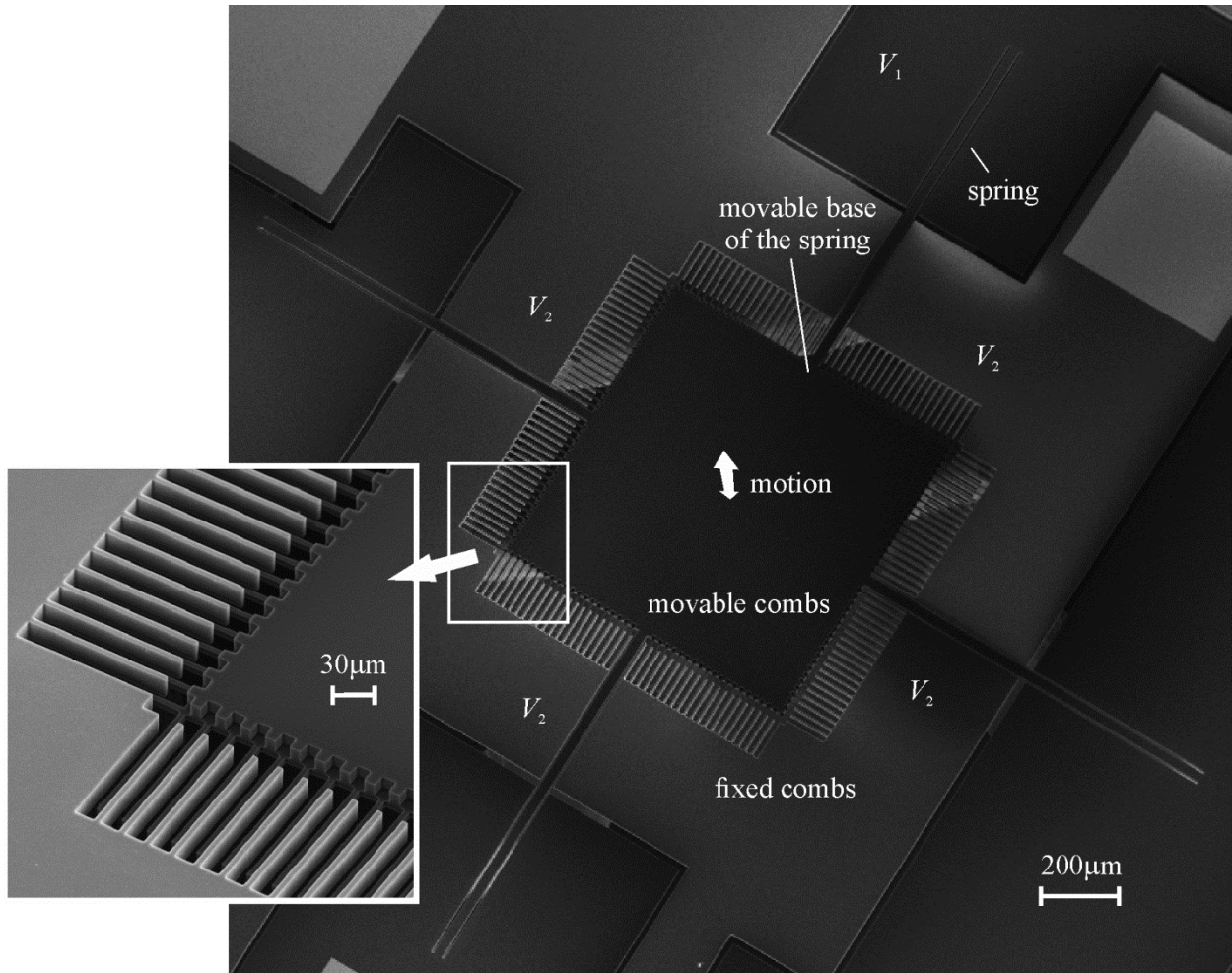


Figure 6.5: The first comb drive fabricated for this study.

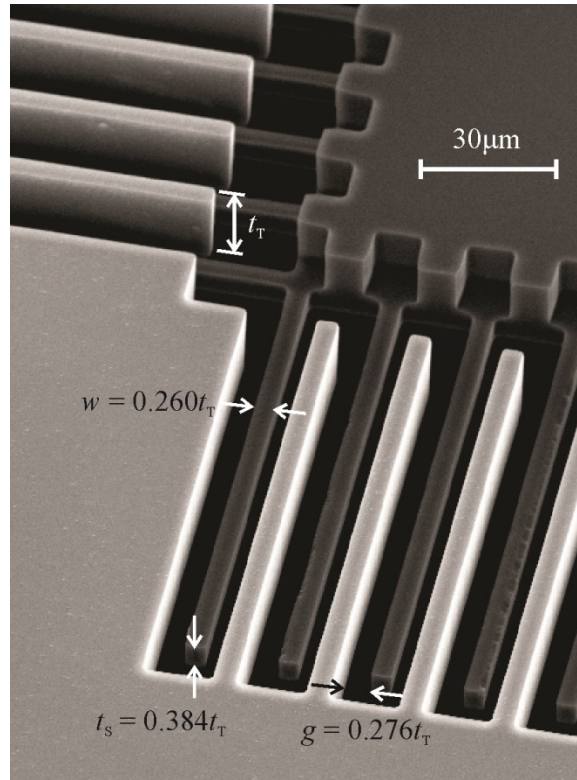


Figure 6.6: The relative tooth dimensions of the comb drive in figure 6.5.

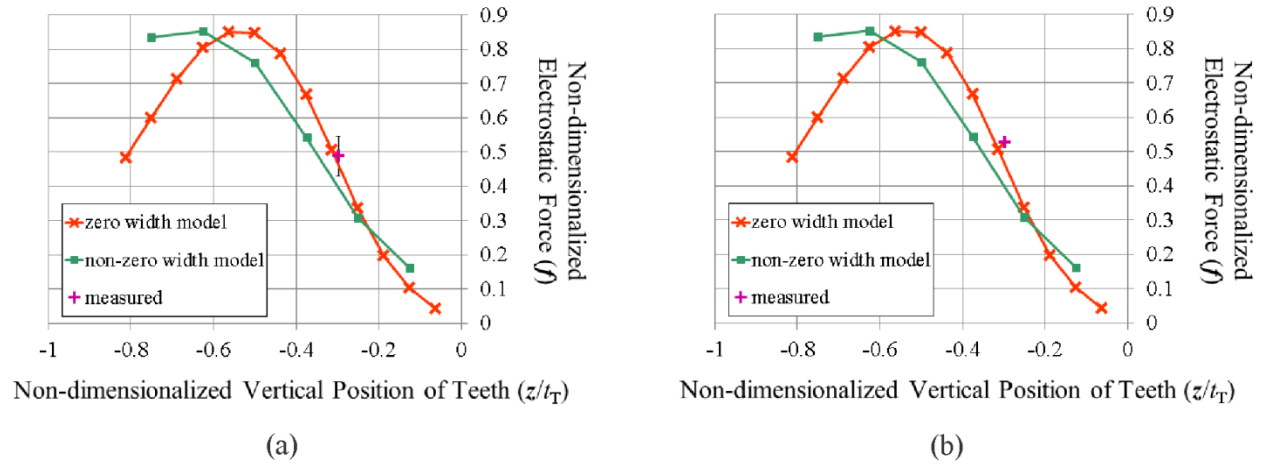


Figure 6.7: A comparison of two different predictions of the electrostatic force to that measured in the vertical comb drive shown in figures 6.5 and 6.6 that has tooth dimensions of  $w/t_T=0.260$ ,  $g/t_T=0.276$ , and  $t_s/t_T=0.384$ . The electrostatic forces have been non-dimensionalized with respect to (6.4). (a) shows the measured force calculated from the spring stiffness determined using the lever mechanism; (b) shows the measured force calculated from the spring stiffness determined with the scale mounted on the stage of the optical profilometer.

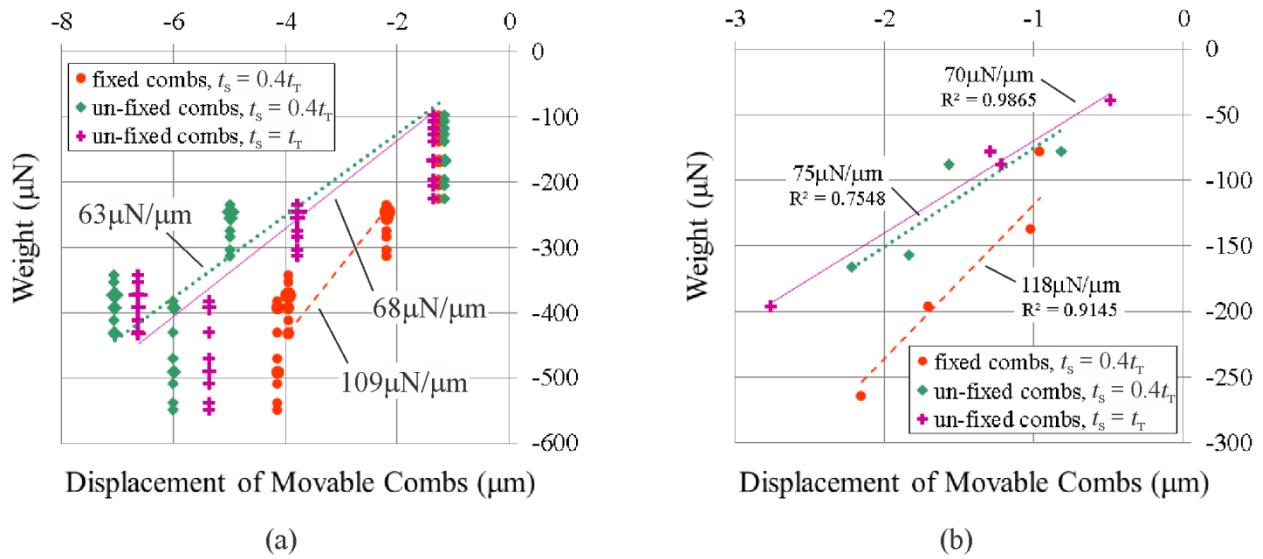


Figure 6.8: The measured spring constants of the three vertical comb drive designs. (a) shows the spring stiffnesses determined using the lever mechanism. A few of the data points have been made larger to indicate that those values of the weights were recorded two or three times. (b) shows the spring stiffness determined with the scale mounted on the stage of the optical profilometer.

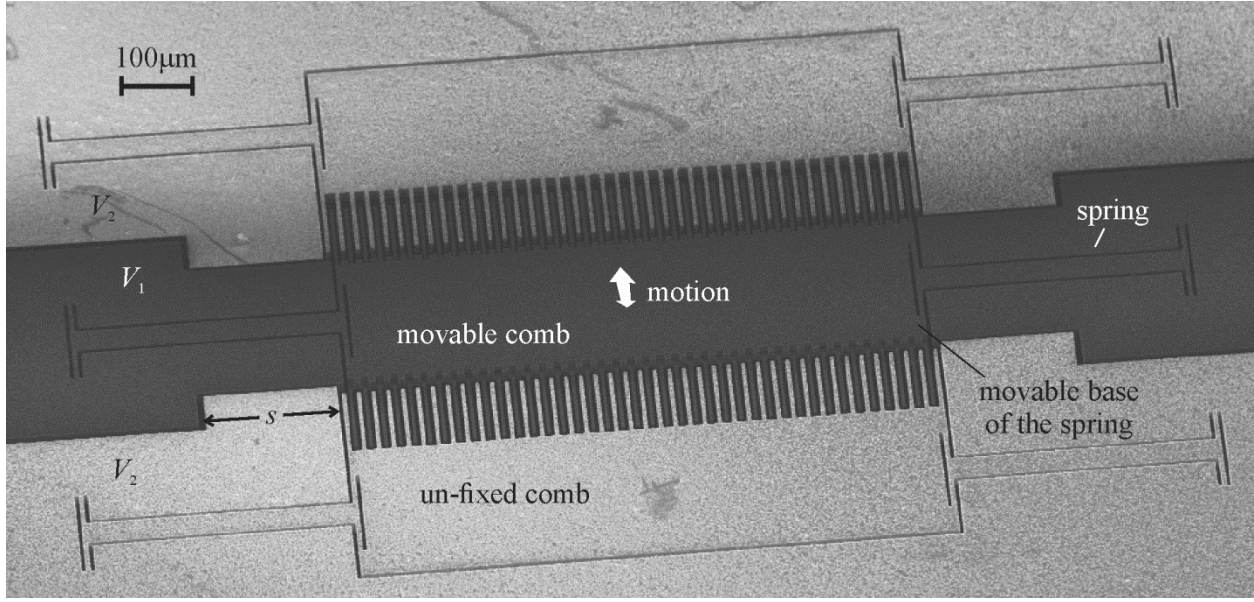


Figure 6.9: The vertical comb drive design that has its “fixed” combs also attached to springs so that they can be pushed down with the electrical probes to allow the electrostatic forces between the fixed and movable teeth to be measured over a larger range of vertical offsets.

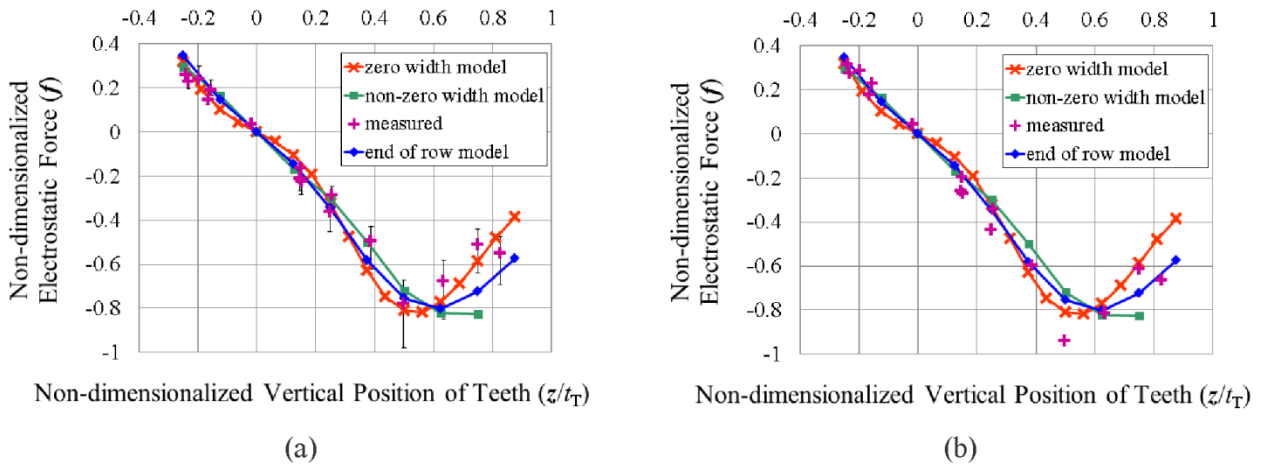


Figure 6.10: Comparisons of three different predictions of the electrostatic forces to those measured in a vertical comb drive that has shorter movable teeth than fixed teeth (with tooth dimensions of  $w/t_1=0.241$ ,  $g/t_1=0.296$ , and  $t_s/t_1=0.365$ ). The electrostatic forces have been non-dimensionalized with respect to (6.4). (a) shows the measured forces calculated from the spring stiffness determined using the lever mechanism; (b) shows the measured forces calculated from the spring stiffness determined with the scale mounted on the stage of the optical profilometer.

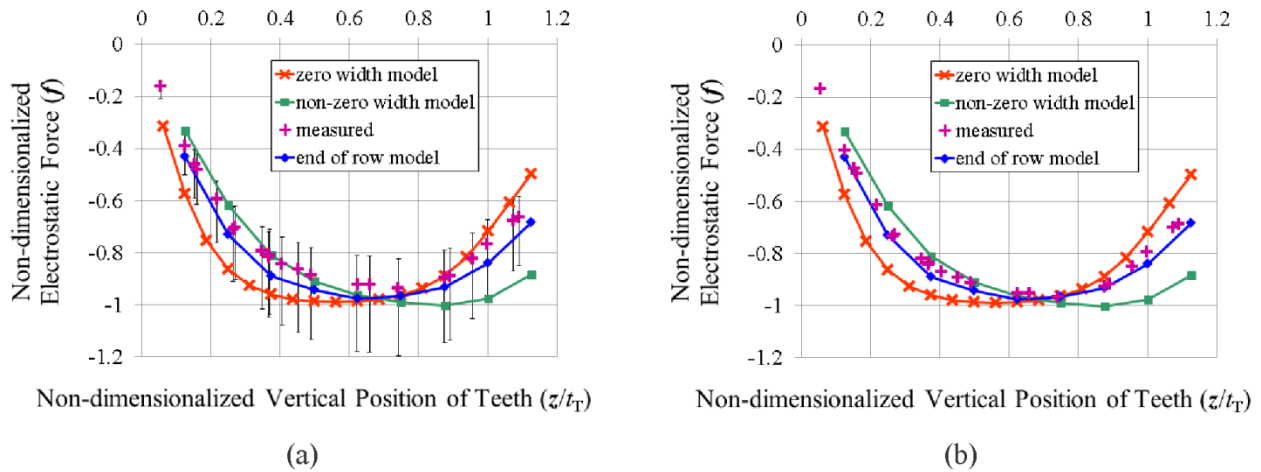


Figure 6.11: Comparisons of three different predictions of the electrostatic forces to those measured in a vertical comb drive that has fixed and movable teeth of the same size ( $w/t_T=0.234$ ,  $g/t_T=0.300$ , and  $t_S/t_T=1$ ). The electrostatic forces have been non-dimensionalized with respect to (6.4). (a) shows the measured forces calculated from the spring stiffness determined using the lever mechanism; (b) shows the measured forces calculated from the spring stiffness determined with the scale mounted on the stage of the optical profilometer.

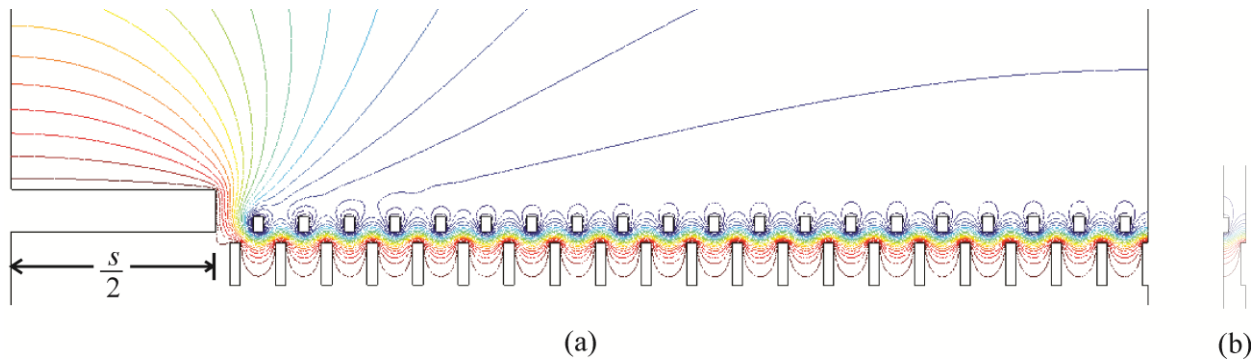


Figure 6.12: (a) One of the models of a row of teeth with a portion of the device layer at the end. The equipotential lines show the electric field being pulled away from the tops of the shorter teeth, lessening the effect of the width of the teeth on the electrostatic force between them. (b) The corresponding unit comb drive.

## Chapter 7 : Conclusions

The overall objective of the research presented here is to begin the design of a comb drive that is to be used as a force-compensation mechanism in an interfacial force microscope. More specifically, the objective of this research is to choose the type of comb drive that has the most potential to further the measurement of interfacial forces, and fabricate test specimens of such comb drives that are then used in two studies that are intended to confirm, at least in part, that comb drives have potential to aid in the measurement of interfacial forces, and to further develop the electrostatic theory used to design comb drives in general. In the first study, the lower limit of the spring stiffness that comb drives can easily be fabricated with is explored, as the mechanical resistance they provide will affect the sensitivity of the force-compensation system. The objective of the second study is to examine how the fringe electric fields around the comb teeth (and thus more of the dimensions of the comb teeth) should be included in the calculation of the electrostatic force between the teeth so that the performance of the comb drives may be predicted more accurately.

Comb drives are an attractive type of force-compensator because they can be made out of common materials and their electrodes can be automatically aligned with each other during their manufacture. This research focuses on comb drives that have springs that are designed to be compliant in the direction perpendicular to the substrate they are machined on (or vertically) rather than in the direction parallel to the substrate (or laterally), as vertically-oriented springs can be fabricated with a lower stiffness more easily. Vertically-offset comb teeth were designed to complement such springs so that electrostatic forces could be applied to the movable combs in both the upwards and downwards directions, and thus both attractive and repulsive interfacial forces on a probe attached to the movable combs could be compensated for. This research further focuses on vertical comb drives that have opposing comb teeth that are offset by a constant amount along their length, without a ground plane, so that a basic geometry can be considered for the modelling of the electric fields around them.

A number of fabrication processes for comb drives that were found in the literature were compared so that the simplest could be chosen that has the capability to produce the type of comb drive required. It was found that a common way for fabrication processes to position the

movable teeth between the fixed teeth in comb drives is to pattern both of their horizontal dimensions with the same mask. It was also realized that with the clever design of the masks, many fabrication processes can produce comb drives capable of not only vertical actuation in both the upwards and downwards directions, but also tilting motions and even horizontal actuation. A simple process that could produce comb drives capable of bi-directional vertical electrical actuation was chosen that created the vertical offset between its combs by etching down the tops of some of their teeth. It was discovered that this could be done using only photoresist to mask the rest of the teeth, which had the advantage of protecting the sides of the teeth as well as their tops during the etch.

By applying loads to the fabricated comb drives through a series of weights and voltages, and measuring the resulting displacements of their movable combs, the stiffnesses of the fabricated springs were calculated to be  $70\mu\text{N}/\mu\text{m}$  ( $64\mu\text{N}/\mu\text{m}$ - $85\mu\text{N}/\mu\text{m}$ ) or  $78\mu\text{N}/\mu\text{m}$ ,  $66\mu\text{N}/\mu\text{m}$  ( $58\mu\text{N}/\mu\text{m}$ - $74\mu\text{N}/\mu\text{m}$ ) or  $64\mu\text{N}/\mu\text{m}$ ,  $6.9\mu\text{N}/\mu\text{m}$  ( $6.2\mu\text{N}/\mu\text{m}$ - $8.1\mu\text{N}/\mu\text{m}$ ) or  $7.2\mu\text{N}/\mu\text{m}$ ,  $6.4\mu\text{N}/\mu\text{m}$  ( $5.7\mu\text{N}/\mu\text{m}$ - $7.5\mu\text{N}/\mu\text{m}$ ) or  $6.7\mu\text{N}/\mu\text{m}$ ,  $0.54\mu\text{N}/\mu\text{m}$  ( $0.48\mu\text{N}/\mu\text{m}$ - $0.63\mu\text{N}/\mu\text{m}$ ) or  $0.56\mu\text{N}/\mu\text{m}$ , and  $0.45\mu\text{N}/\mu\text{m}$  ( $0.40\mu\text{N}/\mu\text{m}$ - $0.52\mu\text{N}/\mu\text{m}$ ) or  $0.46\mu\text{N}/\mu\text{m}$ . The comb drives with the lowest spring stiffnesses are a good first step towards fabricating prototypes that are to aid in measuring interfacial forces.

The net electrostatic force in a vertical comb drive is a function of how the capacitance between its teeth changes with respect to their relative vertical positions. Traditionally, an estimate of the capacitance that does not include the fringe electric fields around the tops and bottoms of the teeth has been used to predict electrostatic forces and choose the dimensions of the teeth. An analytical calculation of the electrostatic force was found in the literature that includes the fringe fields around the tops and bottoms of zero-width teeth, and 2-D finite element models were made of the cross-sections of pairs of teeth to determine the difference the inclusion of their width would make to the prediction of the electrostatic forces. The electrostatic forces predicted with both methods were compared to those measured in fabricated comb drives.

The measured electrostatic forces were found to lie between those predicted with the two different methods, but they seemed to match well with those predicted with 2-D models that were extended to include the cross-sections of the rest of the teeth in the row, as well as a portion of the comb drive at the end of the row. Hence for the ranges of relative heights of the teeth where the width of the teeth is expected to affect the electrostatic force between them, including

a portion of the electrodes around the teeth in the model seems necessary to determine how much the width of the teeth will affect the electrostatic force – as the effect of the width is lessened by the areas around the combs drawing the electric fields away from the tops and bottoms of the teeth.

The measurement of the electrostatic forces in the fabricated comb drives also indicated that the current design will only generate about half of the electrostatic force for any given voltage than that predicted by a model that does not include the fringe fields around the comb teeth. This is something to be aware of when designing for a particular force-voltage relationship in a force-compensation mechanism.

## **7.1 Future Work**

With further models of the electric fields around comb teeth – perhaps three-dimensional models of the ends of the teeth – it could be determined whether including different portions of the electrodes beyond the combs in the models has an effect on the predicted electrostatic force between the combs. Once this is determined, a full parametric study can be conducted to determine the ranges of dimensions and relative vertical positions of the combs where the predictions of the electrostatic forces of the more complex models coincide with those of the simpler models, so that recommendations can be made regarding when the simpler models can be used.

The next step in developing a comb drive to be used as a force-compensation mechanism in an interfacial force microscope is, of course, to adhere a probe in the centre of the movable combs of one of the comb drives fabricated for the studies presented here, and put it in an interfacial force microscope – with a device by which to monitor the displacement of the movable combs, such as an interferometer, and a feedback circuit to supply the voltage to the comb drive and measure the amount of voltage that is being supplied. The sensitivity of such a system can be explored through the imaging of soft material samples. The samples should remain undamaged if the microscope is sensitive enough to detect the interfacial forces close to the sample surface before contacting the surface.

## References

- [1] Selvakumar A and Najafi K 2003 Vertical comb array microactuators *J. MEMS* **12** pp 440-9
- [2] Takahashi K, Mita M, Fujita H and Toshiyoshi H 2006 A high fill-factor comb-driven XY-stage with topological layer switch architecture *IEICE Elec. Exp.* **3** pp 197-202
- [3] Yeh J-L A, Jiang H and Tien N C 1999 Integrated polysilicon and DRIE bulk silicon micromachining for an electrostatic torsional actuator *J. MEMS* **8** pp 456-65
- [4] Krishnamoorthy U, Lee D and Solgaard O 2003 Self-aligned vertical electrostatic combdrives for micromirror actuation *J. MEMS* **12** pp 458-64
- [5] Hah D, Choi C-A, Kim C-K and Jun C-H 2004 A self-aligned vertical comb-drive actuator on an SOI wafer for a 2D scanning micromirror *J. Micromech. Microeng.* **14** pp 1148-56
- [6] Sasaki M, Briand D, Noell W, de Rooij N F and Hane K 2004 Three-dimensional SOI-MEMS constructed by buckled bridges and vertical comb drive actuator *IEEE J. Quantum Electronics* **10** pp 455-61
- [7] Tsai J M-L, Chu H-Y, Hsieh J and Fang W 2004 The BELST II process for a silicon high-aspect-ratio micromachining vertical comb actuator and its applications *J. Micromech. Microeng.* **14** pp 235-41
- [8] Carlen E T, Heng K-H, Bakshi S, Pareek A and Mastrangelo C H 2005 High-aspect ratio vertical comb-drive actuator with small self-aligned finger gaps *J. MEMS* **14** pp 1144-55
- [9] Lin W T, Chiou J C and Tsou C 2005 A self-aligned fabrication method of dual comb drive using multilayers SOI process for optical MEMS applications *Microsys. Tech.* **11** pp 204-9
- [10] Zhang Q X, Liu A Q, Li J and Yu A B 2005 Fabrication technique for microelectromechanical systems vertical comb-drive actuators on a monolithic silicon substrate *J. Vac. Sci. Technol. B* **23** pp 32-41
- [11] Wu M and Fang W 2006 A molded surface-micromachining and bulk etching release (MOSBE) fabrication platform on (111) Si for MOEMS *J. Micromech. Microeng.* **16** pp 260-5
- [12] Wu M and Fang W 2005 Design and fabrication of MEMS devices using the integration of MUMPs, trench-refilled molding, DRIE and bulk silicon etching processes *J. Micromech. Microeng.* **15** pp 535-42
- [13] Iwase E, Onoe H, Matsumoto K and Shimoyama I Hidden vertical comb-drive actuator on PDMS fabricated by parts-transfer *IEEE 21st Int. Conf. on MEMS 2008* (Tucson) pp 116-9
- [14] Kim J, Choo H, Lin L and Muller R S 2006 Microfabricated torsional actuators using self-aligned plastic deformation of silicon *J. MEMS* **15** pp 553-62
- [15] Ko Y-C, Cho J-W, Mun Y-K, Jeong H-G, Choi W K, Kim J-W, Park Y-H, Yoo J-B and Lee J-H 2006 Eye-type scanning mirror with dual vertical combs for laser display *Sens. Actuators A* **126** pp 218-26
- [16] Kim M, Park J-H, Jeon J-A, Yoo B-W, Park I H and Kim Y-K 2009 High fill-factor micromirror array using a self-aligned vertical comb drive actuator with two rotational axes *J. Micromech. Microeng.* **19** pp 1-9

- [17] Kumar K, Hoshino K and Zhang X 2008 Handheld subcellular-resolution single-fibre confocal microscope using high-reflectivity two-axis vertical combdrive silicon microscanner *Biomed. Microdevices* **10** pp 653-60
- [18] Kumar K and Zhang X J CMOS-compatible 2-axis self-aligned vertical comb-driven micromirror for large field-of-view microendoscopes *IEEE 22nd Int. Conf. on MEMS 2009* (Sorrento) pp 1015-8
- [19] Hah D, Choi C-A, Jun C-H and Kim Y T A self-aligned vertical comb-drive actuator using surface micromachining for scanning micromirrors *IEEE/LEOS Int. Conf. on Optical MEMS 2003* pp 151-2
- [20] Chen C, Lee C and Lai Y-J 2003 Novel VOA using in-plane reflective micromirror and off-axis light attenuation *IEEE Comm. Mag.* **41** pp S16-20
- [21] Chung J and Hsu W 2008 Fabrication of a polymer-based torsional vertical comb drive using a double-side partial exposure method *J. Micromech. Microeng.* **18** pp 1-7
- [22] Kouma N, Tsuboi O, Soneda H, Ueda S and Sawaki I Fishbone-shaped vertical comb actuator for dual-axis 1-D analog micromirror array *Transducers 2005* (Seoul) pp 980-3
- [23] Kim J, Park S and Cho D-I 2002 A novel electrostatic vertical actuator fabricated in one homogeneous silicon wafer using extended SBM technology *Sens. Actuators A* **97-98** pp 653-8
- [24] Chan C-K, Hsu C-P, Wu M, Hocheng H, Chen R and Fang W A novel differential capacitive-sensing dual-axis accelerometer design using pendulum-proofmass, gimbal-springs, and HARM vertical-combs *Transducers 2009* (Denver) pp 1944-7
- [25] Tang W C, Nguyen T-U H and Howe R T 1989 Laterally driven polysilicon resonant microstructures *Sens. Actuators* **20** pp 25-32
- [26] Butt H-J, Cappella B and Kappl M 2005 Force measurements with the atomic force microscope: Technique, interpretation and applications *Surf. Sci. Rep.* **59** pp 1-152
- [27] Joyce S A and Houston J E 1991 A new force sensor incorporating force-feedback control for interfacial force microscopy *Rev. Sci. Instrum.* **62** pp 710-5
- [28] Lodge K G 1983 Techniques for the measurement of forces between solids *Adv. in Colloid and Interface Sci.* **19** pp 27-73
- [29] Jarvis S P, Oral A, Weihs T P and Pethica J B 1993 A novel force microscope and point contact probe *Rev. Sci. Instrum.* **64** pp 3515-20
- [30] Jarvis S P, Yamada H, Yamamoto S-I, Tokumoto H and Pethica J B 1996 Direct mechanical measurement of interatomic potentials *Nature* **384** pp 247-9
- [31] Cleveland J, Hansma P and Ducker W 1999 Method and apparatus for magnetic force control of a scanning probe U.S. Patent 5925818
- [32] Lindsay S 1996 Controlled force microscope for operation in liquids U.S. Patent 5515719
- [33] Cleveland J, Hansma P and Ducker W 1997 Method and apparatus for magnetic force control of a scanning probe U.S. Patent 5670712
- [34] Lindsay S, Lyubchenko Y L, Tao N J, Li Y Q, Oden P I, DeRose J A and Pan J 1993 Scanning tunneling microscopy and atomic force microscopy studies of biomaterials at a liquid-solid interface *J. Vac. Sci. Technol. A* **11** pp 808-15
- [35] Yamamoto S, Yamada H and Tokumoto H 1997 Precise force curve detection system with a cantilever controlled by magnetic force feedback *Rev. Sci. Instrum.* **68** pp 4132-6
- [36] Yamamoto S, Yamada H and Tokumoto H 1997 Precise force curves in air and liquid by magnetic force feedback *J. Vac. Sci. Technol. B* **15** pp 1633-6

- [37] Lindsay S and Jing T 2000 Force sensing probe for scanning probe microscopy U.S. Patent 6121611
- [38] Bonander J R and Kim B I 2008 Cantilever based optical interfacial force microscope *Appl. Phys. Lett.* **92** pp 1031241-3
- [39] Kato N, Suzuki I, Kikuta H and Iwata K 1997 Force-balancing microforce sensor with an optical-fibre interferometer *Rev. Sci. Instrum.* **68** pp 2475-8
- [40] Yakimov V and Erlandsson R 2000 Electrostatic force-feedback force sensor incorporated in an ultrahigh vacuum force microscope *Rev. Sci. Instrum.* **71** pp 133-6
- [41] Fretigny C, Michel D, Brocart B and Basire C 2002 Device and method for controlling the interaction of a tip and sample, notably for atomic force microscopy and nano-indentation U.S. Patent 6349591 B1
- [42] Houston J E and Michalske T A 1992 The interfacial-force microscope *Nature Product Review* **356** pp 266-7
- [43] Munoz-Paniagua D J 2004 Development of interfacial force microscopy: applications for materials and interfaces Ph.D. dissertation, Dept. Chemistry, Univ. Western Ontario, London, ON
- [44] Griffith J E and Miller G L 1994 Force-sensing system, including a magnetically mounted rocking element U.S. Patent 5307693
- [45] Miller G L, Griffith J E, Wagner E R and Grigg D A 1991 A rocking beam electrostatic balance for the measurement of small forces *Rev. Sci. Instrum.* **62** pp 705-9
- [46] Grigg D A, Russell P E and Griffith J E 1992 Rocking-beam force-balance approach to atomic force microscopy *Ultramicroscopy* **42-44** pp 1504-8
- [47] Miller S A, Turner K L and MacDonald N C 1999 Drive electrodes for microfabricated torsional cantilevers U.S. Patent 6000280
- [48] Norton P, Dept. of Chemistry, U. of Western Ontario, ON, 2008 Personal Communication
- [49] Munoz-Paniagua D, National Institute for Nanotechnology, AB, 2008 Personal Communication
- [50] Tadayyon S, Dept. of Chemistry, U. of Western Ontario, ON, 2008 Personal Communication
- [51] Chang K-K, Shie N-C, Tai H-M and Chen T-L 2004 A micro force sensor using force-balancing feedback control system and optic-fibre interferometers *Tamkang J. Sci. Eng.* **7** pp 91-4
- [52] Kwon S, Milanovic V and Lee L P 2002 Large-displacement vertical microlens scanner with low driving voltage *Photon. Tech. Lett.* **14** pp 1572-4
- [53] Kim J, Cho D and Muller R S Why is (111) silicon a better mechanical material for MEMS? *Transducers 2001* (Munich) pp 662-5
- [54] Tang W C, Lim M G and Howe R T 1992 Electrostatic comb drive levitation and control method *J. MEMS* **1** pp 170-8
- [55] Ousaid A M, Haliyo S, Regnier S and Hayward V Micro-force sensor by active control of a comb-drive *2013 IEEE/ASME Int. Conf. on AIM* (Wollongong) pp 612-7
- [56] Naftali M and Elata D 2004 Towards a linear response of vertical comb-drive actuators Technical Report ETR-2004-01 Faculty of Mechanical Engineering, Technion, Israel
- [57] Behin B and Pannu S 2004 Multi-layer, self-aligned vertical combdrive electrostatic actuators and fabrication methods U.S. Patent 6744173 B2

- [58] Kwon S, Milanovic V and Lee L P 2004 Vertical combdrive based 2-D gimbaled micromirrors with large static rotation by backside island isolation *IEEE J. Quantum Electronics* **10** pp 498-504
- [59] Milanovic V and Matus G A 2008 Gimbal-less micro-electro-mechanical-system tip-tilt and tip-tilt-piston actuators and a method for forming the same U.S. Patent Application 0061026 A1
- [60] Milanovic V, Matus G A and McCormick D T Tip-tilt-piston actuators for high fill-factor micromirror arrays *Solid-State Sensor, Actuator and Microsystems Workshop 2004* (Hilton Head) pp 232-7
- [61] Choo H, Garmire D, Muller R S and Demmel J 2009 Method for fabricating vertically-offset interdigitated comb actuator device U.S. Patent 7573022 B2
- [62] Choo H, Garmire D, Demmel J and Muller R S 2007 Simple fabrication process for self-aligned, high-performance microscanners - demonstrated use to generate a 2-D ablation pattern *J. MEMS* **16** pp 260-8
- [63] Pilchowski J, Foster M J and Zhou S 2009 Sensor with position-independent drive electrodes in multi-layer silicon on insulator substrate U.S. Patent Application 0025477 A1
- [64] LaFond P H and Yu L 2008 MEMS vertical comb drive with improved vibration performance U.S. Patent 7469588 B2
- [65] Milanovic V 2004 Multilevel beam SOI-MEMS fabrication and applications *J. MEMS* **13** pp 19-30
- [66] Madou M J 2002 *Fundamentals of Microfabrication: The Science of Miniaturization*, 2nd ed. (Boca Raton, FL: CRC Press) pp 285
- [67] Kim J, Christensen D and Lin L 2006 Micro vertical comb actuators by selective stiction process *Sens. Actuators A* **127** pp 248-54
- [68] Lee D, Krishnamoorthy U, Yu K and Solgaard O 2004 Single-crystalline silicon micromirrors actuated by self-aligned vertical electrostatic combdrives with piston-motion and rotation capability *Sens. Actuators A* **114** pp 423-8
- [69] Carr E, Olivier S and Solgaard O Large-stroke self-aligned vertical comb drive actuators for adaptive optics applications *SPIE 6113: MEMS/MOEMS Components and Their Applications III 2006* pp 0T1-9
- [70] Wada H, Lee D, Krishnamoorthy U, Zappe S and Solgaard O 2002 Process for high speed Micro Electro Mechanical Systems (MEMS) scanning mirrors with vertical comb drives *Jpn. J. Appl. Phys.* **41** pp L899-901
- [71] Tsou C, Lin W T, Fan C C and Chou B C S 2005 A novel self-aligned vertical electrostatic combdrives actuator for scanning micromirrors *J. Micromech. Microeng.* **15** pp 855-60
- [72] Cho J-W, *et al.* Electrostatic 1D micro scanner with vertical combs for HD resolution display *SPIE 6466: MOEMS and Miniaturized Systems VI 2007* pp 0B1-12
- [73] Hamaguchi H, Sugano K, Tsuchiya T and Tabata O A differential capacitive three-axis SOI accelerometer using vertical comb electrodes *Transducers 2007* (Lyon) pp 1483-6
- [74] Zickar M, Mita M, Ataka M and Fujita H 2007 Low cross talk design and simple fabrication process of electrostatic vertical comb-drive actuators for positioning application *IEEJ Trans.* **2** pp 289-94
- [75] Tsuchiya T and Funabashi H 2004 A z-axis differential capacitive SOI accelerometer with vertical comb electrodes *Sens. Actuators A* **116** pp 378-83

- [76] Yang Z, Wang C, Yan G, Hao Y and Wu G A bulk micromachined lateral axis gyroscope with vertical sensing comb capacitors *Transducers 2005* (Seoul) pp 121-4
- [77] Liu X, Yang Z, Yan G, Fan J, Ding H and Liu Y Design and fabrication of a lateral axis gyroscope with asymmetric comb-fingers as sensing capacitors *1st IEEE Int. Conf. Nano/Micro Engineered and Molecular Systems 2006* (Zhuhai) pp 762-5
- [78] Lee J-H, Ko Y-C, Choi B-S, Kim J-M and Jeon D Y 2002 Bonding of silicon scanning mirror having vertical comb fingers *J. Micromech. Microeng.* **12** pp 644-9
- [79] Wu B, Kumar A and Pamarthy S 2010 High aspect ratio silicon etch: A review *J. Appl. Phys.* **108** pp (051101)1-20
- [80] Young W C and Budynas R G 2002 *Roark's Formulas for Stress and Strain*, 7th ed. (New York: McGraw-Hill) ch 10
- [81] Zickar M, Mita M, Ataka M and Fujita H 2007 Low cross talk design and simple fabrication process of electrostatic vertical comb-drive actuators for positioning application *IEEJ Trans* **2** pp 289-94
- [82] Halliday D, Resnick R and Walker J 1997 *Fundamentals of Physics - Extended*, 5th ed. (New York: Wiley) pp 629-37
- [83] Legtenberg R, Groeneveld A W and Elwenspoek M 1996 Comb-drive actuators for large displacements *J. Micromech. Microeng.* **6** pp 320-9
- [84] Liu C 2006 *Foundations of MEMS* (Upper Saddle River, NJ: Pearson Prentice Hall) pp 133-4
- [85] Palmer H B 1937 The capacitance of a parallel-plate capacitor by the Schwarz-Christoffel transformation *Trans. Amer. Inst. Elec. Eng.* **56** pp 363-6
- [86] Koc C K and Ordnung P F 1989 Schwarz-Christoffel transformation for the simulation of two-dimensional capacitance [VLSI circuits] *IEEE Trans. Comp. Des. Int. Circ.* **8** pp 1025-7
- [87] Nussbaum A 1995 Capacitance and spreading resistance of a stripe line *Solid-State Elec.* **38** pp 1253-6
- [88] Yeh J-L A, Hui C-Y and Tien N C 2000 Electrostatic model for an asymmetric combdrive *J. MEMS* **9** pp 126-35
- [89] Hui C-Y, Yeh J-L A and Tien N C 2000 Calculation of electrostatic forces and torques in MEMS using path-independent integrals *J. Micromech. Microeng.* **10** pp 477-82
- [90] Gradshteyn I S and Ryzhik I M 2000 *Table of Integrals, Series, and Products*, 6th ed. (San Diego: Academic Press) pp 851-2